Global Biogeochemical Cycles

RESEARCH ARTICLE
10.1029/2024GB008164

Feedbacks From Young Permafrost Carbon Remobilization to the Deglacial Methane Rise

M. Sabino[1,2], Ö. Gustafsson[3], B. Wild[3,4], I. P. Semiletov[5,6], O. V. Dudarev[5,6], G. Ingrosso[7], and T. Tesi[1]

[1]Institute of Polar Sciences, National Research Council, Bologna, Italy, [2]Joint Research Center ENI-CNR Aldo Pontremoli, Lecce, Italy, [3]Department of Environmental Science, Stockholm University, Stockholm, Sweden, [4]Bolin Centre for Climate Research, Stockholm University, Stockholm, Sweden, [5]V.I. Il'ichev Pacific Oceanological Institute (POI), Russian Academy of Sciences, Far Eastern Branch, Vladivostok, Russia, [6]Tomsk State University (TSU), Tomsk, Russia, [7]Research Institute on Terrestrial Ecosystems, National Research Council, Lecce, Italy

Key Points:

- A few thousand years old permafrost organic carbon (OC) was massively remobilized from East Siberian soils during the Preboreal climate transition
- Remineralization of a few thousand years old OC may increase the maximum allowable deglacial methane emissions from permafrost
- Age complexities of permafrost OC must be considered to better constrain the permafrost carbon-climate feedback

Supporting Information:

Supporting Information may be found in the online version of this article.

Correspondence to:

M. Sabino,
sabinomathia@gmail.com;
mathia.sabino@isp.cnr.it

Citation:

Sabino, M., Gustafsson, Ö., Wild, B., Semiletov, I. P., Dudarev, O. V., Ingrosso, G., & Tesi, T. (2024). Feedbacks from young permafrost carbon remobilization to the deglacial methane rise. *Global Biogeochemical Cycles*, *38*, e2024GB008164. https://doi.org/10.1029/2024GB008164

Received 12 MAR 2024
Accepted 5 SEP 2024

Author Contributions:

Conceptualization: M. Sabino, Ö. Gustafsson, T. Tesi
Data curation: M. Sabino
Formal analysis: M. Sabino
Funding acquisition: Ö. Gustafsson, B. Wild, I. P. Semiletov, T. Tesi
Investigation: M. Sabino, G. Ingrosso
Methodology: M. Sabino, T. Tesi
Project administration: Ö. Gustafsson, T. Tesi
Resources: Ö. Gustafsson, B. Wild, I. P. Semiletov, T. Tesi
Software: M. Sabino
Supervision: Ö. Gustafsson, T. Tesi
Visualization: M. Sabino

Abstract The abrupt warming events punctuating the Termination 1 (about 11.7–18 ka Before Present, BP) were marked by sharp rises in the concentration of atmospheric methane (CH_4). The role of permafrost organic carbon (OC) in these rises is still debated, with studies based on top-down measurements of radiocarbon (^{14}C) content of CH_4 trapped in ice cores suggesting minimum contributions from old and strongly ^{14}C-depleted permafrost OC. However, organic matter from permafrost can exhibit a continuum of ^{14}C ages (contemporaneous to >50 ky). Here, we investigate the large-scale permafrost remobilization at the Younger Dryas-Preboreal transition (ca. 11.6 ka BP) using the sedimentary record deposited at the Lena River paleo-outlet (Arctic Ocean) to reflect permafrost destabilization in this vast drainage basin. Terrestrial OC was isolated from sediments and characterized geochemically measuring $\delta^{13}C$, $\Delta^{14}C$, and lignin phenol molecular fossils. Results indicate massive remobilization of relatively young (about 2,600 years) permafrost OC from inland Siberia after abrupt warming triggered severe active layer deepening. Methane emissions from this young fraction of permafrost OC contributed to the deglacial CH_4 rise. This study stresses that underestimating permafrost complexities may affect our comprehension of the deglacial permafrost OC-climate feedback and helps understand how modern permafrost systems may react to rapid warming events, including enhanced CH_4 emissions that would amplify anthropogenic climate change.

Plain Language Summary Feedback on climate change through methane emissions from organic carbon (OC) released from thawing permafrost soils is still debated. Studies investigating rapid warming events from the last 15,000 years and measuring the radiocarbon content in methane from ancient air trapped in ice cores suggested small contributions from the oldest (10,000 years or more) and most refractory OC fraction to the deglacial methane rise. However, the younger and more reactive OC likely contributed more to methane emissions from permafrost systems. Using terrestrial material from sediments deposited at the paleo-delta of the Lena River (Arctic Ocean), we investigated large-scale permafrost OC remobilization across the climate transition to the Preboreal (about 11,600 years ago). Results show that relatively young (about 2,600 years) terrestrial organic matter was largely remobilized from the layer of East Siberian permafrost soils thawing seasonally that deepened fast due to abrupt warming. Using the young radiocarbon age of remobilized permafrost OC established in this study suggests that permafrost systems might have contributed more than previously thought to the deglacial methane rise. Considering more components of the heterogeneous permafrost OC pool will be crucial to better constrain past and future impacts on climate change.

1. Introduction

The ongoing Arctic warming is destabilizing high latitude permafrost soils (Meredith et al., 2019), reintroducing previously frozen organic matter into the modern carbon cycle (ICCI, 2023; Schuur et al., 2015). This makes permafrost organic carbon (OC) vulnerable to microbial degradation, causing emissions of greenhouse gases (GHGs) into the atmosphere (Dean et al., 2018). In particular, methane (CH_4) emissions are receiving increasing attention (ICCI, 2023; Meredith et al., 2019). However, to what extent CH_4 is released from thawing permafrost is still poorly constrained because of the limited knowledge on the dynamics of permafrost reactivation (Smith et al., 2022; Turetsky et al., 2020), the dominant type of OC released (Martens et al., 2022), and the hydrological cycle (Andresen et al., 2020) that collectively drive CH_4 production and release. Because of the higher warming

Writing – original draft: M. Sabino
Writing – review & editing: M. Sabino, Ö. Gustafsson, B. Wild, I. P. Semiletov, O. V. Dudarev, G. Ingrosso, T. Tesi

potential of CH_4, improved constraints of the permafrost OC-climate feedback through CH_4 emissions is a priority and a challenge in climate change science. To this end, rapid warming events from the near geological past may offer valuable insights into climate feedbacks from thawing permafrost.

The Termination 1 (T1; about 11.7–18 thousand years Before Present, BP; Denton et al., 2010) coincided with a global climate reorganization, with an average temperature rise of 6–7°C (Osman et al., 2021). Estimates from models suggest that deglacial warming caused massive release of terrestrial OC from Arctic permafrost (up to 1,000 Pg C; Pg = 10^{15} g; Ciais et al., 2012; Lindgren et al., 2018) through various reactivation pathways (e.g., Jones et al., 2023). For instance, erosion of coastal permafrost has remobilized deep and ancient carbon pools (Martens et al., 2019, 2020; Meyer et al., 2019; Winterfeld et al., 2018). However, not only ancient carbon pools were remobilized. In fact, further evidence demonstrates that moderately pre-aged material was also reactivated through active layer deepening triggered by warming (Tesi, Muschitiello, et al., 2016). Simultaneously to the massive permafrost OC release, the atmospheric CH_4 concentration rose by about 330 nmol/mol with two abrupt increase events at about 14.6 and 11.6 ka BP (Köhler et al., 2017). The contribution of permafrost OC to this rise is still debated.

Different remobilization processes have implications for the emissions of GHGs, ultimately controlling their radiocarbon ($\Delta^{14}C$) fingerprint and ^{14}C age. In this respect, studies based on $\Delta^{14}C$ measurements of atmospheric CH_4 from ice cores have questioned the importance of old sources such as ancient permafrost OC in the deglacial CH_4 budget (Dyonisius et al., 2020; Petrenko et al., 2017). Although their outcomes do not exclude a young permafrost OC source per se, the authors suggest that contemporaneous terrestrial organic matter (terrOM) recycled in tropical wetlands was instead the dominant source controlling deglacial atmospheric CH_4 variability. This was remarked by recent investigations on differences in CH_4 concentration between Greenland and Antarctic ice cores (Riddell-Young et al., 2023). Although those studies provide constraints on the contributions from old permafrost OC to the deglacial CH_4 rise, top-down estimates from $^{14}CH_4$ (e.g., Dyonisius et al., 2020; Petrenko et al., 2017) do not strongly constrain substantial remobilization of younger OC during permafrost thaw. In fact, even today, evidence from the modern Arctic reveals a great heterogeneity in permafrost OC composition and decomposability (i.e., reactive continuum; Bröder et al., 2016), with different processes releasing OC with ages ranging from contemporaneous (same $\Delta^{14}C$ value as atmospheric CO_2) to late Pleistocene ($\Delta^{14}C \approx -1{,}000‰$; Grosse et al., 2011; Guo et al., 2004; Gustafsson et al., 2011; Martens et al., 2022; Vonk et al., 2012).

Terrestrial OM transported from Arctic rivers carries a signal that traces spatial and temporal dynamics of permafrost OC release from vast inland domains in response to climate perturbations (e.g., Guo et al., 2007; Semiletov et al., 2011; Wild et al., 2019; X. Zhang et al., 2017). Therefore, the particulate OC fraction depositing in prodelta sediments is a suitable tool to resolve the dominant release mechanisms and disentangle the contribution of deep versus shallow sources. By examining the riverine OC fraction deposited in shallow settings and utilizing the watershed of great Arctic rivers as a natural spatial integrator, we can better understand the comprehensive response of extensive inland permafrost regions to climate change.

In this study, we assess whether young permafrost OC could have contributed to the deglacial atmospheric CH_4 rise targeting a paleo-outlet river setting. Specifically, we follow up on the study of Tesi, Muschitiello, et al. (2016) who investigated bulk sediment OC (OC_{bulk}) from a piston core record deposited on the Laptev Sea shelf (Arctic Ocean) at the Lena River paleo-outlet (site piston core 23 (PC23), Figure 1). The depositional setting is ideal because it receives abundant terrestrial material from the extensive Lena catchment (Martens et al., 2021, 2022; McClelland et al., 2016; Winterfeld, Goñi, et al., 2015), thus reflecting large scale remobilization of organic matter from the largest Arctic watershed draining a continuous permafrost domain (Amon et al., 2012). Additionally, X-ray images revealed that sediments are highly laminated, indicating rapid deposition and negligible post-depositional transport (Tesi, Muschitiello, et al., 2016). These factors contribute to minimize the potential ^{14}C age difference between CH_4 emitted from permafrost systems and terrestrial OC released from permafrost and ultimately trapped in marine sediments. The latter may in fact experience extensive redistribution and aging during cross-shelf transport (Matsubara et al., 2022; Tesi, Semiletov, et al., 2016), which in the Arctic shelves may last up to a few thousands of years (Bröder et al., 2018). In particular, we focus on the Younger Dryas-Preboreal (YD-PB; ca. 11.6 ka BP) transition, when rapid warming at the end of T1 coincided with the sharpest increase in atmospheric CH_4 (ca. 275 nmol/mol; Köhler et al., 2017). Previous results from OC_{bulk} suggest that terrOM deposited during the transition was moderately pre-aged ($\Delta^{14}C_{OCbulk} = -203‰$ to $-313‰$) and mainly came from the sub-surface of Arctic soils (Tesi, Muschitiello, et al., 2016). While remobilization of permafrost

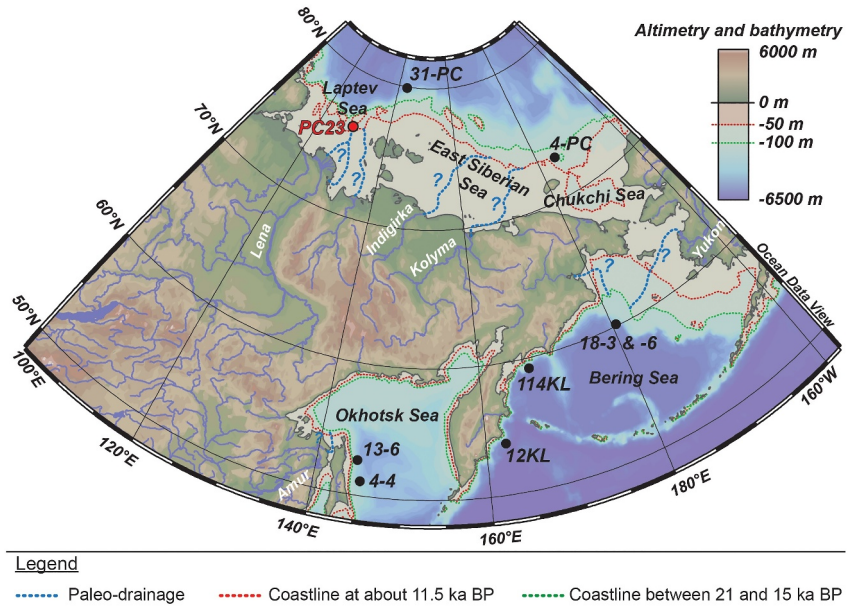

Figure 1. Map created using Ocean Data View (Schlitzer, 2023) showing the location of Piston Core 23 (PC23; Tesi, Muschitello, et al., 2016) and other sediment cores discussed for comparison in this study (31-PC: Martens et al., 2020; 4-PC: Martens et al., 2019; 18-3 and -6, 114KL, 12KL: Meyer et al., 2019; 13-6, 4-4: Winterfeld et al., 2018). Paleo-drainage above and below 70°N according to Martens et al. (2019, 2020) and Meyer et al. (2019), respectively.

OC through coastal erosion cannot be responsible for CH_4 production, the latter can occur after gradual thawing of permafrost soils (Dean et al., 2018), implying potential CH_4 emissions during rapid climate transitions.

To address our research question, we specifically targeted particulate terrOM from the low density (LD; <1.8 g/cm^3) sediment fraction. Organic carbon from the LD fraction (OC_{LDf}) may account for up to 50% of OC_{bulk} in coastal settings (Tesi, Semiletov, et al., 2016), making it highly representative of the type and dynamics of permafrost OC released after thawing. Working with OC_{LDf} helps overcome ^{14}C age bias toward specific pools of the permafrost OC estimated through terrestrial biomarkers (e.g., leaf wax lipids; Winterfeld et al., 2018) that account for a minimal fraction of the overall OC_{bulk} (i.e., <1%). The OC_{LDf} is also composed of large plant fragments that rapidly accumulate off prodeltas (e.g., Wakeham et al., 2009), thus experiencing minimal across-shelf transport that typically affects fine minerals (Bröder et al., 2018; Tesi, Semiletov, et al., 2016). We focused on these coarse (≥63 μm) particles to represent the biospheric contribution and to minimize potential influence from soot, petrogenic OC (Dickens et al., 2004) and phytoplankton remains, which contribute to OC_{bulk} (Tesi, Muschitello, et al., 2016). All these sources can collectively affect $\Delta^{14}C$ of OC_{bulk}, hampering the precise determination of the ^{14}C age of OC remobilized from Arctic soils and, consequently, infer the $\Delta^{14}C$ signature of CH_4 emissions.

Here, we used the $\Delta^{14}C$ fingerprint of OC_{LDf} to accurately determine the age of terrOM and to apportion the OC pools (shallow/young vs. deep/old) in combination with measurements of stable C isotopes ($\delta^{13}C$) and biomarker analyses (lignin phenols) to further characterize the source of terrOM. We then compared our results with studies on permafrost OC remobilization during T1 published elsewhere. Finally, we estimated potential CH_4 emissions from thawing inland permafrost during T1, based on our observed ^{14}C age of remobilized OC, using the same approach as Dyonisius et al. (2020). Evidence from this study suggests that implementing the complexity of permafrost OC may improve our understanding of the permafrost OC-climate feedback, which will help to adopt appropriate strategies to mitigate the consequences of anthropogenic climate change.

2. Materials and Methods

2.1. Sediment Samples and Study Area

Marine sediments used in this study are from the 4.02 m-long PC23 previously described in detail by Tesi, Muschitiello, et al. (2016). The core was retrieved in 2014 in the mid/outer-shelf of the Laptev Sea (Lat 76°

10.26′N, Long 129° 20.22′E, water depth of about 56 m; Figure 1) during the joint expedition SWERUS-C3 (Swedish-Russian-U.S. Arctic Ocean—Investigation of Climate-Cryosphere-Carbon interactions). The sediments are represented from bottom to top core by 1.3 m of homogeneous sand, 2.5 m of laminated mud (providing samples investigated in this study), and 23 cm of homogeneous mud, the latter deposited under fully marine conditions (Tesi, Muschitiello, et al., 2016).

The Laptev Sea is the shallowest epicontinental sea of the Arctic Ocean (on average 48 m deep, Figure 1; Jakobsson et al., 2004). Its continental shelf is cut by elongated submarine paleo-valleys carved by rivers during the last glacial period and subsequently partially filled by sediments during the late Pleistocene-Holocene transgression (Bauch & Kassens, 2005; Bauch et al., 2001; Taldenkova et al., 2008). Sediments supplied to the Laptev Sea derive from coastal erosion of Pleistocene Ice Complex deposits and riverine input from the Lena River (Winterfeld, Goñi, et al., 2015).

The Lena River catchment is among the largest in the Arctic with an area of 2.46 km^2 (Amon et al., 2012). About 90% of it is currently underlain by permafrost (Brown et al., 1997; T. Zhang et al., 2005) that is topped by a seasonally thawing active layer few centimeters to several meters thick (T. Zhang et al., 2005). The climate is extremely continental, with short hot summers (up to +35°C), long cold winters (−50°C on average), and low mean annual precipitation (up to 500 mm; Chevychelov & Bosikov, 2010; Winterfeld, Goñi, et al., 2015). Most of the Lena catchment is occupied by forests with species typical of the boreal and taiga zones, while tundra vegetation is restricted to the North (Amon et al., 2012; Chevychelov & Bosikov, 2010). During the Last Glacial Maximum and T1, the area occupied by permafrost was larger (Lindgren et al., 2016) and the overall climate was cooler and drier (Andreev et al., 2011; Biskaborn et al., 2016; Kostrova et al., 2021). Open tundra-steppe vegetation dominated the watershed, with arboreal species confined to *refugia* and expanding only during the short episodes of pronounced climate amelioration until they took over starting from the late Holocene (Ashastina et al., 2017; Baumer et al., 2021; Tarasov et al., 2009).

2.2. Chronology

The age-depth model for PC23 was developed by Tesi, Muschitiello, et al. (2016) using 14 samples (11 marine fossil shells and three large plant fragments) ^{14}C dated at the US-NSF National Ocean Sciences Accelerator Mass Spectrometry facility at Woods Hole Oceanographic Institution (Woods Hole, MA, USA). Modeling was performed using OxCal (version 4.2; Bronk Ramsey, 2008, 2009) and the marine and terrestrial ^{14}C age calibration curves from 2013 (Marine13 and IntCal13, respectively; Reimer et al., 2013). According to the model from Tesi, Muschitiello, et al. (2016), sediments encompass the entire YD-PB transition and the Holocene. Following the same approach, we revise the age-depth model using the latest calibration curves (Marine20 and IntCal20, respectively; Heaton et al., 2020; Reimer et al., 2020) and version (4.4.4) of the OxCal software (Text S1 in Supporting Information S1). Furthermore, we assess the reliability of our updated age-depth model (and indirectly of the original model proposed by Tesi, Muschitiello, et al., 2016) through the approximate approach recently proposed by Heaton et al. (2023) for age models from polar regions encompassing glacial periods (Text S1 in Supporting Information S1). Applying such corrections produced no significant improvement in the updated (and original) chronology. Furthermore, the comparison between the original and updated results shows that the ages obtained for sediment deposition at the level corresponding to the 14 samples are virtually identical, with differences well within the uncertainty associated with the modeled date for each sample. Because the methane emission model applied in this study (see Section 2.7) was built using IntCal13 (cf. Dyonisius et al., 2020), we opted for the age-depth model proposed by Tesi, Muschitiello, et al. (2016), which further scored a higher agreement index (94.6%) than the updated model (82.7%; Text S1 in Supporting Information S1). This choice allows for internal consistency with the methane emission model and for comparison with literature results. We encourage using our updated age-depth model based on the more advanced, latest ^{14}C calibration curves for future studies, and remark that the choice we made does not compromise the outcome of this work. In fact, the closeness of the age-depth models implies that it would be possible to apply either of the two models coming to analogous conclusions for this study.

2.3. Isolation of the Low-Density (LD) Fraction and Microscope Observations

About 9 g of freeze-dried bulk sediment for each sample was fractionated by density using an aqueous solution of sodium metatungstate monohydrate (Sigma-Aldrich) and setting the density cutoff to 1.8 g/cm^3 (Wakeham

et al., 2009). Sediment samples were placed into 45 mL centrifuge tubes, which were filled with the solution, bringing the sediment in suspension with a vortex mixer. The tubes were then left in a rack for about 15 min before centrifugation at 3,000 rpm for 20 min to separate the low-density (LD, <1.8 g/cm^3) and high density (HD, >1.8 g/cm^3) fractions. The supernatant and the LD fraction in suspension were poured onto a 0.45 µm polyvinylidene difluoride (PVDF) membrane filter and the tubes were gently washed with the sodium metatungstate solution to collect the LD fraction sticking on the tube walls. The procedure was repeated (up to 6 times) until the supernatant was clear. The PVDF filters carrying the LD fractions were then transferred into new 45 mL centrifuge tubes which were filled with MilliQ water and sonicated for 2 min. The tubes were left in a rack for 30 min before centrifugation at 3,000 rpm for 15 min to let the LD fraction settle down. Each LD fraction was rinsed 3 times with MilliQ water to remove the sodium monotungstate, every time settling down the LD fraction with the centrifuge (3,000 rpm/15 min) before pipetting away the supernatant from the tubes. The same procedure was followed for the HD fractions left in the tubes to get rid of the sodium monotungstate, rinsing the HD fraction 3 times in total. Both fractions were then freeze dried and no further analyses were performed on the HD fractions.

The LD fractions were then inspected through an optical microscope and at high resolution with an environmental scanning electron microscope Zeiss EVO LS 10, equipped with an Energy-Dispersive Spectroscopy device Bruker (Quantax system; Esprit software) at the Institute of Microelectronics and Microsystems from the National Research Council of Italy (Bologna Section). The latter instrument was further used to take digital images working in high vacuum conditions and using a backscattered detector at 15kV. Visual inspection revealed traces of fine minerals left in the suspension and collected during sediment fractionation. We wet-sieved ($\phi = 63$ µm) the LD fractions with MilliQ water to avoid contribution from soot (e.g., Tesi, Semiletov, et al., 2016), petrogenic C (e.g., Dickens et al., 2004), and/or phytoplankton. The Δ^{14}C fingerprint from these C sources overlaps with permafrost OC (e.g., Vonk et al., 2012), hampering the precise determination of the ^{14}C age of remobilized permafrost OC and hence inferring CH_4 emissions from this source. Meanwhile, sieving concentrated the non-mineral bound part of permafrost OC, which is most vulnerable to microbial degradation after thawing (e.g., Gentsch et al., 2018; Wang et al., 2023).

2.4. Total Organic Carbon (OC), Stable Carbon Isotopes (δ^{13}C) and Biomarker Analyses

Total OC content and δ^{13}C analyses were performed on an aliquot of each LD fraction using a Thermo DeltaQ isotope-ratio mass spectrometer coupled to a Thermo Flash 2000 Elemental Analyzer via a ConFlo IV interface after acidification (Ag capsules, HCl, 1.5 M) to remove inorganic carbon (Nieuwenhuize et al., 1994). Results are reported in Table S2 in Supporting Information S1 as weight percentage (wt.%). The δ^{13}C values are expressed in the conventional delta notation (‰) ad reported in Table 1. Based on replicates of in-house standards, the standard deviation was lower than ±0.15‰.

Biomarker analyses focused on phenol monomers (Goñi & Hedges, 1995; Hedges & Mann, 1979) released from the LD fractions after applying alkaline cupric oxide (CuO) oxidation according to Goñi and Montgomery (2000). Analyses were carried out in the organic chemistry laboratories of the Joint Research Center ENI-CNR-"Aldo Pontremoli" (Lecce, Italy). Depending on the OC content, 2–3 mg of each LD fraction was loaded in Teflon tubes with CuO and ammonium iron (II) sulfate hexahydrate [$(NH_4)_2Fe(SO_4)_2 \cdot 6H_2O$]. Everything was brought in suspension in a solution of N_2-purged NaOH (2 N) and the oxidation was performed in oxygen-free conditions at 150°C for 90 min in a Microwave Accelerated Reaction System 5 from CEM. A known amount of ethylvanillin was added as recovery standard to the solutions after the oxidation step. The aqueous solutions were then acidified to pH 1 with HCl (12 N) and extracted with ethyl acetate. Finally, the extracts were dried and redissolved in pyridine. After derivatization with bis(trimethylsilyl) trifluoroacetamide +1% trimethylchlorosilane at 60°C for 30 min, the CuO oxidation products were quantified using an Agilent 7890A gas chromatograph (GC) coupled to an Agilent 5975C MS in full scan mode (50–650 *m/z*). The GC system was equipped with an Agilent DB1-MS capillary column (60 m × 250 µm; 0.25 µm film thickness). The following temperature program was applied: initial temperature of 100°C and hold for 1 min, from 100 to 290°C at 4°C min^{-1}, then hold at 290°C for 10 min. The target compounds were quantified using the response factors of commercially available standards. Lignin-derived reaction products include vanillyl phenols (V = vanillin, Vl; acetovanillone, Vn; vanillic acid, Vd), syringyl phenols (S = syringealdehyde, Sl; acetosyringone, Sn; syringic acid, Sd) and cinnamyl phenols (C = *p*-coumaric acid, pCd; ferulic acid, Fd). Additionally, the 3,5-dihydroxybenzoic acid (3,5-Bd) and *p*-hydroxy phenols (P = *p*-hydroxyacetophenone, Pn; *p*-hydroxybenzaldehyde, Pl; *p*-hydroxybenzoic acid, Pd) were measured. Results are presented in Table S2 in Supporting Information S1 as ratios of OC-normalized data.

Table 1
Stable Carbon Isotopes ($\delta^{13}C$), Radiogenic Carbon Isotopes at Time of Deposition ($\Delta^{14}C_i$), and Pre-Depositional ^{14}C Ages (Pre-Dep.) With Associated Errors (1σ) for Organic Carbon From Low-Density Fractions (OC_{LDf}; This Work) and Bulk Sediments (OC_{bulk}; Tesi, Muschitiello, et al., 2016)

				OC_{LDf} (this work)			OC_{bulk} (Tesi, Muschitiello, et al., 2016)		
Sample ID PC23	Depth (cm)	Age of sediment deposition (Cal. BP)	2σ age of sediment deposition (Cal. BP)	$\delta^{13}C$ (‰)	$\Delta^{14}C_i \pm 1\sigma$ (‰)	Pre-dep. ^{14}C age ± 1σ (years)	$\delta^{13}C$ (‰)	$\Delta^{14}C_i \pm 1\sigma$ (‰)	Pre-dep. ^{14}C age ± 1σ (years)
I_0-1	0.5	−33	−71 to 471	−26.2	−819.0 ± 3.9	15,401 ± 178	−23.9	−429.9 ± 11.6	–
I_28-29	28.5	11,140	11,064–11,209	−27.1	−228.7 ± 8.7	3,244 ± 92	−26.3	−307.8 ± 4.6	4,113 ± 55
I_43-44	43.5	11,193	11,131–11,254	−27.1	−228.7 ± 6.1	3,228 ± 65	−26.3	−301.8 ± 4.3	4,027 ± 52
I_63-64	63.5	11,246	11,187–11,310	−27.2	−188.2 ± 6.2	2,740 ± 63	−26.3	−289.5 ± 4.6	3,811 ± 55
I_94-95	94.5	11,326	11,255–11,398	−27.2	−228.7 ± 6.4	3,139 ± 69	−26.7	−279.1 ± 5.3	3,682 ± 62
II_10-11	124.5	11,402	11,306–11,486	−27.2	−184.6 ± 8.4	2,714 ± 84	−26.4	–	–
II_48-49	162.5	11,499	11,370–11,596	−27.3	−173.8 ± 7.9	2,674 ± 78	−26.6	−253.9 ± 6.7	3,494 ± 72
II_81-82	195.5	11,588	11,432–11,699	−27.4	−70.6 ± 9.3	1,838 ± 82	−26.9	−196.7 ± 7.8	3,009 ± 80
II_103-104	217.5	11,646	11,472–11,764	−27.5	−75.4 ± 9.9	1,863 ± 88	−26.7	−199.9 ± 8.1	3,025 ± 83
II_120-121	234.5	11,692	11,497–11,817	−27.5	−98.8 ± 11.2	2,129 ± 102	−26.5	−237.9 ± 8.5	3,476 ± 91
Average				*−27.3*	*−164.2*	*2,618.9*	*−26.5*	*−258.3*	*3,579.6*
1σ				*0.2*	*65.7*	*556.9*	*0.2*	*43.7*	*414.1*

Note. Note that average values exclude the top core sample (0.5 cm) and that $\Delta^{14}C_i$ for OC_{bulk} were updated according to the procedure followed in this work. Pre-dep. ^{14}C ages for OC_{bulk} represent possible minimum ages assuming a 100% contribution from plant material (source apportionment from Tesi, Muschitiello, et al. (2016) indicates that marine organic matter contributed between 11% and 22% to OC_{bulk}). Cal. BP: calibrated years Before Present (=1950 AD).

2.5. Radiocarbon Isotope Analyses, ^{14}C Ages, and Calibrated ^{14}C Ages

Depending on the OC content, 4–7 mg of each LD fraction was sent to the US-NSF National Ocean Sciences Accelerator Mass Spectrometry facility at Woods Hole Oceanographic Institution (Woods Hole, MA, USA) for ^{14}C content measurement and subsequent dating. Before shipment, the sub-samples were acidified with HCl (1.5 M) to remove the carbonate fraction, rinsed with MilliQ water, and finally dried at the organic chemistry laboratories of the Joint Research Center ENI-CNR-"Aldo Pontremoli" (Lecce). The absolute amount of ^{14}C in the sample at the time of measurement accounting for decay of both the sample and the standard since 1950 AD has been reported according to Stuiver and Polach (1977) as:

$$\Delta^{14}C = \left[Fm \times e^{\lambda(1950-Yc)} - 1\right] \times 1{,}000\ (‰) \quad (1)$$

where Fm indicates the Fraction modern (expressed as the ratio of $^{14}C/^{12}C_{sample}$ and $^{14}C/^{12}C_{standard}$, the former normalized to $\delta^{13}C = -25‰$ and the latter (oxalic acid I) normalized to $\delta^{13}C = -19‰$ and corrected for decay by multiplying by 0.95 to equal the pre-industrial ^{14}C content in 1890), λ is the decay constant based on Cambridge half-life (1/8,267 yr^{-1}), and *Yc* is the year of collection (as AD) of the sample. The $\Delta^{14}C$ values from the LD fractions are reported in Table S3 in Supporting Information S1.

Radiocarbon ages were calculated from $\delta^{13}C$-corrected Fm according to the formula:

$$^{14}Cage = -8{,}033 \times \ln(Fm) \quad (2)$$

where −8,033 represents the mean lifetime of ^{14}C. Values are reported following convention (Stuiver & Polach, 1977) in Table S3 in Supporting Information S1. Radiocarbon ages were calibrated against the atmospheric curve IntCal13 (Reimer et al., 2013) according to the adopted age model using OxCal (v. 4.4.4). Using IntCal13 is justified by microscope observations and $\delta^{13}C$ values, both indicating that plant debris represent organic matter from the LD fractions (see Section 3). Calibrated ^{14}C dates are shown in Table S3 in Supporting Information S1.

2.6. Calculation of $\Delta^{14}C$ at Time of Deposition ($\Delta^{14}C_i$) and Pre-Depositional ^{14}C Ages

To calculate $\Delta^{14}C_i$, we followed Nogarotto et al. (2023) using the $\Delta^{14}C$ values reported in Table S3 in Supporting Information S1 and the equation:

$$\Delta^{14}C_i = \left[\left(\frac{\Delta^{14}C}{1{,}000} + 1\right) \times e^{\lambda t} - 1\right] \times 1{,}000\ (‰) \tag{3}$$

where $\lambda = 1/8{,}267\ yr^{-1}$ and t is the time of deposition of the corresponding sediment interval according to the chronology of PC23.

Using $\Delta^{14}C_i$ values and again following Nogarotto et al. (2023), we extrapolated the pre-depositional ^{14}C ages applying the formula:

$$\text{pre-depositional } ^{14}C \text{ age} = -8{,}033 \times \ln\left(\frac{1 + \frac{\Delta^{14}C_i}{1{,}000}}{1 + \frac{\Delta^{14}C_{atm}}{1{,}000}}\right) \tag{4}$$

where $\Delta^{14}C_{atm}$ is the atmospheric $\Delta^{14}C$ at time of sediment interval deposition estimated from the IntCal13 data set (Reimer et al., 2013) for consistency with the age-depth model, and from direct atmospheric measurements for the modern (core top) sample (Hua et al., 2013). To estimate uncertainty on $\Delta^{14}C_i$ and pre-depositional ^{14}C ages, Gaussian propagation error was applied (http://www.julianibus.de/) using errors associated to the $\Delta^{14}C$ values, the time of deposition from the age-depth model, and the $\Delta^{14}C_{atm}$ as input data. Results are reposted in Table 1.

2.7. Modeling of Methane Emissions

To estimate emissions of CH_4 from organic matter released from permafrost, we applied the one-box model inversion from Dyonisius et al. (2020), which provide a detailed description of the method in their Supplementary Material. Briefly, at first the model uses CH_4 mole fraction data from the NEEM (Rosen, 2014) and WAIS (Buizert et al., 2015) ice cores to calculate the total atmospheric CH_4 burden (M_{atm}, Tg CH_4, Tg = 10^{12} g) and global emissions (Q_{tot} Tg CH_4/yr) assuming a lifetime for atmospheric CH_4 (τ) of about 10.05 years (Dyonisius et al., 2020). Thereafter, we estimated contributions to the deglacial CH_4 emissions from permafrost OC following the assumption that all ^{14}C-depleted CH_4 released into the atmosphere derive from this source. The ^{14}C isotopic mass balance for atmospheric CH_4 implies that

$$^{14}C_{atm}(t) = f_p \times {}^{14}C_p(t) + (1 - f_p) \times {}^{14}C_{IntCal}(t) \tag{5}$$

where $^{14}C_{atm}$ corresponds to the ^{14}C content of atmospheric CH_4 (i.e., $\Delta^{14}CH_4$), f_p is the fraction of atmospheric CH_4 burden coming from permafrost, $^{14}C_p$ is the ^{14}C activity of CH_4 emitted at time t by permafrost OC (mainly deriving from the active layer OC pool up to 1 m depth in our scenario), and $^{14}C_{IntCal}$ is the ^{14}C activity of contemporaneous atmospheric $^{14}CO_2$ from the IntCal13 data set (according to Dyonisius et al., 2020) at the same time t; the ^{14}C terms are expressed as age-corrected percent modern carbon.

Using the ^{14}C age we obtained for permafrost OC (on average 2,619 ± 557 years), the term $^{14}C_p$ at the time of emission (t) was calculated as follows:

$$^{14}C_p(t) = {}^{14}C_{IntCal}(t + 2{,}619 \pm 557) \times e^{-\lambda(2{,}619 \pm 557)} \tag{6}$$

where λ equals $1/8{,}267\ yr^{-1}$. Solving Equation 5 for f_p to obtain the fraction of atmospheric burden from permafrost OC, the model uses f_p to calculate the amount of atmospheric CH_4 burden coming from permafrost OC emissions (M_p) at time t as:

$$M_p(t) = f_p \times M_{atm}(t) \tag{7}$$

Table 2
Modeled Methane Emissions (Mean and 95% Confidence Intervals, CI) Released From Permafrost Organic Carbon Assuming an Old (7,500 ± 2,500 years) End Member (, Dyonisius et al., 2020) and Young (2,619 ± 557 years) End Member (This Study)*

		CH_4 emissions from old OC (Tg CH_4/yr)*				CH_4 emissions from young OC (Tg CH_4/yr)			
		Full distribution		Physical realizations		Full distribution		Physical realizations	
Sample ID	Age (Cal BP)	Mean	95% CI	Mean	95% CI	Mean	95% CI	Mean	95% CI
Oldest Dryas 1	14,920	*−6*	−54 to **29**	12	0–42	*−20*	−112 to **62**	26	1–85
Oldest Dryas 2	14,860	*−4*	−55 to **24**	11	0–40	*−26*	−118 to **50**	22	1–76
Transition 1	14,580	*0*	−54 to **25**	11	0–40	*−23*	−116 to **57**	23	1–81
Transition 2	14,540	*1*	−52 to **21**	10	0–31	*−26*	−115 to **47**	21	1–71
Bølling 2	14,420	*4*	−31 to **42**	16	1–48	*13*	−69 to **101**	33	1–106
Bølling 1	14,420	*11*	−26 to **53**	18	1–57	*23*	−58 to **121**	39	2–119
Allerød	13,000	*−6*	−51 to **18**	9	0–32	*−25*	−94 to **38**	18	1–62
Younger Dryas 1	11,715	*−6*	−37 to **24**	10	0–34	*−10*	−70 to **44**	18	1–59
Transition 1	11,559	*11*	−15 to **42**	15	1–43	*22*	−28 to **79**	28	2–82
Transition 2	11,515	*12*	−15 to **43**	15	1–44	*18*	−28 to **80**	28	2–79
Preboreal 1	11,453	*−2*	−35 to **32**	12	0–37	*0*	−67 to **62**	24	1–70
Preboreal 2	11,357	*2*	−25 to **35**	13	0–38	*6*	−52 to **72**	25	1–81
10.2k sample #1	10,130	*−5*	−27 to **25**	10	0–31	*−1*	−53 to **50**	19	1–62
10.2k sample #2	10,130	*−5*	−33 to **19**	8	0–30	*−10*	−68 to **37**	16	1–52
9.2k sample	9,210	*−19*	−55 to **5**	7	0–22	*−40*	−107 to **9**	12	0–43
8.2k sample	7,940	*−4*	−39 to **23**	9	0–29	*−9*	−71 to **42**	17	1–54

Note. Following Dyonisius et al. (2020), we report emissions both from the full and only the physical parts of the Monte Carlo error propagations highlighting in italics (mean) and bold (upper limit for CH_4 emissions from permafrost) values most relevant for the discussion. Sample ages are from Dyonisius et al. (2020) and Petrenko et al. (2017). Tg = 10^{12} g.

Finally, the magnitude of CH_4 emissions from permafrost (Q_p, Tg CH_4/yr) is estimated by the model solving for Q_p the differential equation:

$$\frac{d(M_p)}{dt} = Q_p - k \times M_p \quad (8)$$

and using a steady-state approximation for M_p ($dM_p/dt = 0$), where $k = 1/\tau$ ($\tau = 10.05$). Following Dyonisius et al. (2020), we further calculated CH_4 emissions that are physically possible, namely CH_4 emissions for which $0 < f_p < 1$ ($f_p < 0$ gives negative CH_4 emissions while $f_p > 1$ implies that $^{14}C_p$ is greater than $^{14}C_{atm}$). Methane emissions during the YD-PB transition were obtained running anew the original model, which included data from Petrenko et al. (2017), not shown in Dyonisius et al. (2020). Results for the time intervals shown by Dyonisius et al. (2020) and Petrenko et al. (2017) are reported in Table 2 along with the original estimates from the publications for a comparison.

3. Results and Discussion

3.1. Terrestrial Material Mobilized From East Siberian Inland Permafrost in the Latest Termination 1

Scanning electron microscope observations on LD fractions show that terrOM deposited at the Lena River paleo-outlet across the YD-PB transition (11.1–11.7 ka BP) is composed of plant debris (Figure 2a) with no evidence of algal material. Ratios of carbon stable isotopes (Table 1) support this origin, indicating that the material derived from C_3 plants (from −35‰ to −20‰; Hedges et al., 1997; Tipple & Pagani, 2007) is the dominant vegetation at Arctic latitudes (Körner et al., 1991; Kristensen et al., 2011). Moreover, $\delta^{13}C$ values indicate negligible

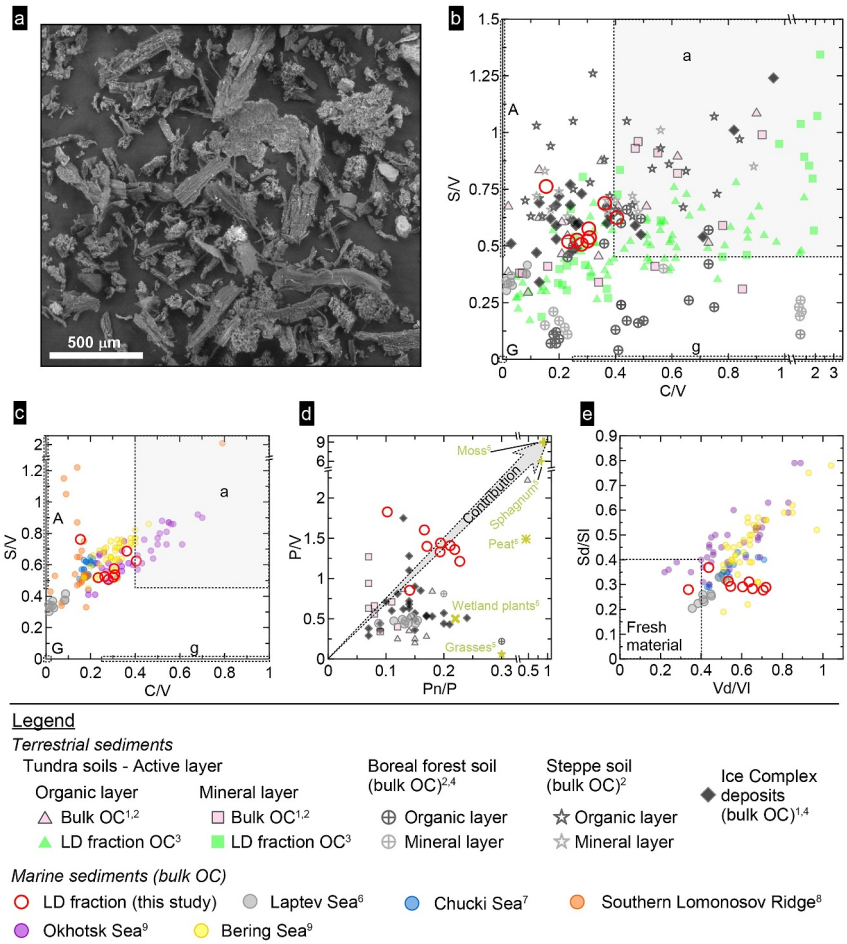

Figure 2. Close up view of the terrestrial material investigated in this study, and vegetation and degradation proxies based on cupric oxide oxidation products. (a) Scanning electron microphotograph of a representative sample of low density fraction. (b, c) Vegetation-source parameters for vascular plants. (d) Vegetation-source parameters used to detect contribution from mosses. (e) Degradation indices for terrestrial organic matter. Literature values: (1) Tesi et al. (2014); (2) Dao et al. (2023); (3) Dao et al. (2022); (4) Winterfeld, Goñi, et al. (2015); (5) Table 4 in Amon et al. (2012) and references therein; (6) Tesi, Muschitiello, et al. (2016), (7) Martens et al. (2019); (8) Martens et al. (2020); (9) Cao et al. (2023). Note that to allow for comparison we selected the same samples (or the closest ones when data were unavailable) for six and only samples from the early deglacial to the Preboreal (9–19.1 ky BP) for 7 to 9. Compositional ranges in (b) and (c) from Winterfeld, Goñi, et al. (2015). A: woody angiosperms; a: non-woody angiosperms; C: cinnamyl phenols; G: woody gymnosperms; g: non-woody gymnosperms; OC: organic carbon; P: *p*-hydroxybenzene phenols; Pn: *p*-hydroxyacetophenone; S: syringyl phenols; Sd: syringic acid; Sl: syringealdehyde; V: vanillyl phenols; Vd: vanillic acid; Vl: vanillin.

contribution from riverine plankton, otherwise expected to result in $\delta^{13}C \leq -29‰$ (Winterfeld, Laepple, & Mollenhauer, 2015 and references therein). We used biomarkers (phenolic compounds) to discriminate the main vegetation source of plant debris, together with radiocarbon ($\Delta^{14}C$) dating to identify where the material stemmed from (shallow/young vs. deep/old permafrost OC pool).

3.1.1. Phenolic Monomers Trace Terrestrial Plant Inputs and Degradation State

Phenolic monomers allow to constrain the vegetation source of terrOM delivered to the marine realm (e.g., Prahl et al., 1994; Winterfeld, Goñi, et al., 2015 and references therein) and to evaluate its degradation state due to pre- and post-depositional diagenetic processes (Hedges & Prahl, 1993; Matsubara et al., 2022 and references therein).

Relative contribution from vascular plants to vegetation remains from the LD fractions was assessed through ratios between syringyl (S), vanillyl (V), and cinnamyl (C) phenols, which allowed discriminating between woody and non-woody tissues from angiosperms and gymnosperms (Goñi & Hedges, 1995; Hedges &

Mann, 1979; Hedges et al., 1997). The S/V and C/V ratios indicate a greater contribution from non-woody tissues of Arctic angiosperm plants than from tissues of gymnosperms (Table S2 in Supporting Information S1; Figure 2b). This inference is supported by the greater affinity with the phenolic fingerprint of terrestrial OC from the active layer of modern tundra soils (Dao et al., 2022; Tesi et al., 2014) and steppe soils (Dao et al., 2023) rather than boreal forest soils (Amon et al., 2012; Figure 2b). Overlap with the lignin fingerprint of terrOM enclosed in Siberian Ice Complex deposits (Figure 2b) and remobilized during T1 to the Arctic Ocean and northernmost Pacific Ocean (Figure 2c) further support our inference. In fact, terrOM enclosed in Ice Complex deposits is largely represented by remains from grasslands, meadow steppes, and shrub tundra from the late Pleistocene tundra-steppe flora (e.g., Andreev et al., 2011; Ashastina et al., 2017, 2018; Strauss et al., 2017), that was identified as the main source of terrOM remobilized during T1 (Cao et al., 2023; Martens et al., 2019, 2020). These observations confirm that the vascular plant debris from our LD fractions were mostly derived from angiosperms forming the Pleistocene tundra-steppe flora, which endured in East Siberia until the Early Holocene (Andreev et al., 2011; Ashastina et al., 2017, 2018; Strauss et al., 2017). This material was delivered to the Lena River paleo-outlet together with organic matter derived from woody gymnosperms (Tesi, Muschitiello, et al., 2016). Comparison with OC_{bulk} (Figure 2b) indicates that the latter was largely adsorbed to the HD (>1.8 g/cm^3) mineral fraction, likely due to partitioning of terrOM between sediment fractions (e.g., Bergamaschi et al., 1997; Keil et al., 1998; Wakeham et al., 2009). Because boreal forests persisted only in *refugia* in the Lena watershed throughout T1 (Kobe et al., 2022; Tarasov et al., 2013), this mineral-bound OC may derive from the erosion of pre-LGM paleo-soils, when forests were more widespread (Andreev et al., 2011; Zech et al., 2010). Lower $\Delta^{14}C$ values of OC_{bulk} (Tesi, Muschitiello, et al., 2016) than OC_{LDf} support this inference (Table S3 in Supporting Information S1).

Contributions of non-vascular plants (mosses, such as *Sphagnum*) to our LD fractions were evaluated through ratios between *p*-hydroxybenzene phenols (P), *p*-hydroxyacetophenone (Pn), and vanillyl phenols (e.g., Amon et al., 2012; Dickens et al., 2011; Williams et al., 1998). The P/V and Pn/P values suggest contribution from non-vascular plants to our samples (Figure 2d; Table S2 in Supporting Information S1). This is supported by P/V ratios close to organic matter from peatlands (Williams et al., 1998) and by P/V and Pn/P ratios greater than most values from OC_{bulk} reported for the modern active layer and Ice Complex deposits from northeastern Siberia (Figure 2d), all typified by low contribution from mosses (Tesi et al., 2014). Furthermore, the end of T1 coincided with the onset of the rapid expansion of peatlands and wetlands across the Arctic (MacDonald et al., 2006; Nichols & Peteet, 2019; Treat et al., 2019, 2021), hinting at overall wetter conditions presumably more conducive to the growth of mosses. Contributions from non-vascular plants to terrOM remobilized from the Lena watershed across the YD-PB transition went unnoticed from previous observations on OC_{bulk} (Figure 2d; Tesi, Muschitiello, et al., 2016) and may support increasing wetness of permafrost soils.

To constrain the degradation state of OC from the LD fraction we applied ratios between syringic acid (Sd) and syringealdehyde (Sl), vanillic acid (Vd), and vanillin (Vl), and the 3,5-dihydroxybenzoic acid (3,5-Bd) and vanillyl (V) phenols, whose values increase as oxic degradation of organic matter proceeds (Benner et al., 1990; Opsahl & Benner, 1995; Otto & Simpson, 2006). The Sd/Sl, Vd/Vl, and 3,5-Bd/V ratios (Figure 2d; Table S2 in Supporting Information S1; av. 3,5-Bd/$V_{LD} = 0.09 \pm 0.02$) of terrOM from the LD fractions are low, in agreement with previous findings on OC_{bulk} (Tesi, Muschitiello, et al., 2016; Figure 2d). This indicates that independently from the sediment fraction, terrOM from PC23 sediments experienced little oxic degradation before and after deposition. The likely reasons were fast translocation to the Laptev Sea shelf, and rapid settling and minimal redistribution processes within the shelf (e.g., Bröder et al., 2016; Tesi, Semiletov, et al., 2016). Little degradation is further confirmed by the comparison (Figure 2d) with terrOM remobilized during T1 and deposited offshoreward (Figure 1), which experienced greater redistribution and cross-shelf transport (Cao et al., 2023; Martens et al., 2019).

In summary, vascular plant debris delivered to the Lena River paleo-delta across the YD-PB transition was derived from vegetation typical of the late Pleistocene tundra-steppe flora. Organic carbon from gymnosperm woody plants and non-vascular plants entered the paleo-coastal sector of the Laptev Sea too, the former largely adsorbed on the heavy mineral fraction. Terrestrial organic matter was rapidly transported from inland East Siberia to the Laptev Sea shelf experiencing limited pre- and post-depositional oxic degradation.

3.1.2. Radiocarbon Constraints on the Age and Provenance of the Plant Debris

The ^{14}C content of OC released from Arctic soils allows to determine its age and hence its provenance within the highly heterogeneous permafrost OC pool (e.g., Grosse et al., 2011; Guo et al., 2004; Martens et al., 2022; Tesi et al., 2014; Wild et al., 2019). In general, the topsoil and the active layer (up to 1 m depth) store a mixture of contemporaneous and moderately pre-aged (a few thousand years old) terrOM from the sub-surface resulting in moderately ^{14}C-depleted $\Delta^{14}C$ values (Figure 3a). Conversely, mostly tens of thousands of years old OC is stored in deeper permafrost layers exhibiting strongly ^{14}C-depleted to ^{14}C-dead $\Delta^{14}C$ values (Figure 3a). Building on these differences observed in the modern Arctic, multiple studies have used ^{14}C ages to discriminate the source of terrestrial OC released to the Arctic and northernmost Pacific Oceans throughout T1 and beyond (Martens et al., 2019, 2020; Meyer et al., 2019; Tesi, Muschitiello, et al., 2016; Winterfeld et al., 2018).

Radiocarbon measurements on the OC_{LDf} show that the land-derived material is strongly ^{14}C-depleted (av. $-790‰ \pm 12‰$; Table S3 in Supporting Information S1), corresponding to a mean calibrated age of 14,735 years BP (Table S3 in Supporting Information S1). These results are in line with previous findings on OC_{bulk} (Tesi, Muschitiello, et al., 2016), which appear slightly more ^{14}C-depleted (av. $-814‰ \pm 7‰$; Table S3 in Supporting Information S1). To reconstruct the ^{14}C content and age of organic matter at the time when it was trapped in marine sediments ($\Delta^{14}C_i$ and pre-depositional ^{14}C age, respectively), the time elapsed since sediment deposition and the composition of atmospheric $^{14}CO_2$ must be considered (see Section 2). Applying these corrections, we obtained that the plant debris were scarcely ^{14}C-depleted (av. $\Delta^{14}C_i = -164‰ \pm 66‰$; Table 1 and Figure 3a) when deposited at the Lena River paleo-outflow, appearing about 100‰ less ^{14}C-depleted than OC_{bulk} (av. $\Delta^{14}C_i = -258‰ \pm 44‰$, Table 1; Tesi, Muschitiello, et al., 2016). Translating $\Delta^{14}C_i$ values into pre-depositional ^{14}C ages revealed that terrOM translocated from inland East Siberia had an average pre-depositional ^{14}C age of 2,619 ± 557 years (Table 1; Figure 3b), about 1,000 ^{14}C years younger than the possible minimum pre-depositional ^{14}C age estimated from OC_{bulk} (av. 3,580 ± 414 years; Table 1; Tesi, Muschitiello, et al., 2016). These results indicate that plant debris was derived from vegetation growing few millennia before the YD-PB transition in the Lena watershed, while OC_{bulk} also included older organic matter that was adsorbed to the mineral fraction. Assuming that the OC pool of deglacial and modern permafrost systems shared an analogous structure, these data support that much of the terrOM from PC23 samples stemmed from the shallow (0–1 m) OC pool within the Lena catchment (Figure 3a). According to the scenario proposed by Tesi, Muschitiello, et al. (2016), the terrestrial material was massively remobilized from inland East Siberia following fast warming at the YD-PB transition, which triggered rapid thickening of the thin active layer, in turn likely promoting localized superficial erosion events (e.g., active layer detachment slides, thermal erosion gullies, and retrogressive thaw slumps; Bröder et al., 2021; Grosse et al., 2011; Turetsky et al., 2020). Washing off and rapid translocation to the Laptev Sea of the destabilized material was then favored by enhanced riverine runoff, probably connected to overall wetter conditions in central Asia (Katsuta et al., 2018; Steffensen et al., 2008; Tarasov et al., 2009) and intensified water discharge from accelerated permafrost thawing (Katsuta et al., 2019).

Insights from ^{14}C analyses of OC_{LDf} reveal that relatively young (av. 2,619 ± 557 years) terrestrial OC was released from the shallow sub-surface of soils within the Lena catchment across the YD-PB transition. We propose that fast climate warming accompanying the transition triggered the widespread remobilization of this material through rapid thickening of the active layer, further promoting thermokarst development releasing older mineral-bound OC. Because active layer OC was shown to have a greater potential to be emitted as CH_4 at the site of thaw than OC from the underlying permafrost (Treat et al., 2015), its widespread remobilization might have promoted CH_4 emissions to the atmosphere.

3.2. Complexities of Late Deglacial Permafrost Systems

Here, we put observations from our study site in a broader time-space perspective by comparing them with evidence from other sediment records from the Arctic Ocean and the northernmost Pacific Ocean (Figure 1), all indicating remobilization of permafrost OC during the late phase of T1 (<15 ka BP; Martens et al., 2019, 2020; Meyer et al., 2019; Winterfeld et al., 2018). The comparison highlights the complexities of late deglacial permafrost systems.

Bulk sediment OC data from the Southern Lomonosov Ridge (Martens et al., 2020; Figure 1) and the Chukchi Sea shelf (Martens et al., 2019; Figure 1) indicate increasing terrOM input from inland East Siberia and Beringia since about 15 ka BP. The ^{14}C-depleted $\Delta^{14}C$ signature of OC_{bulk} (Figure 3a) revealed that terrOM derived

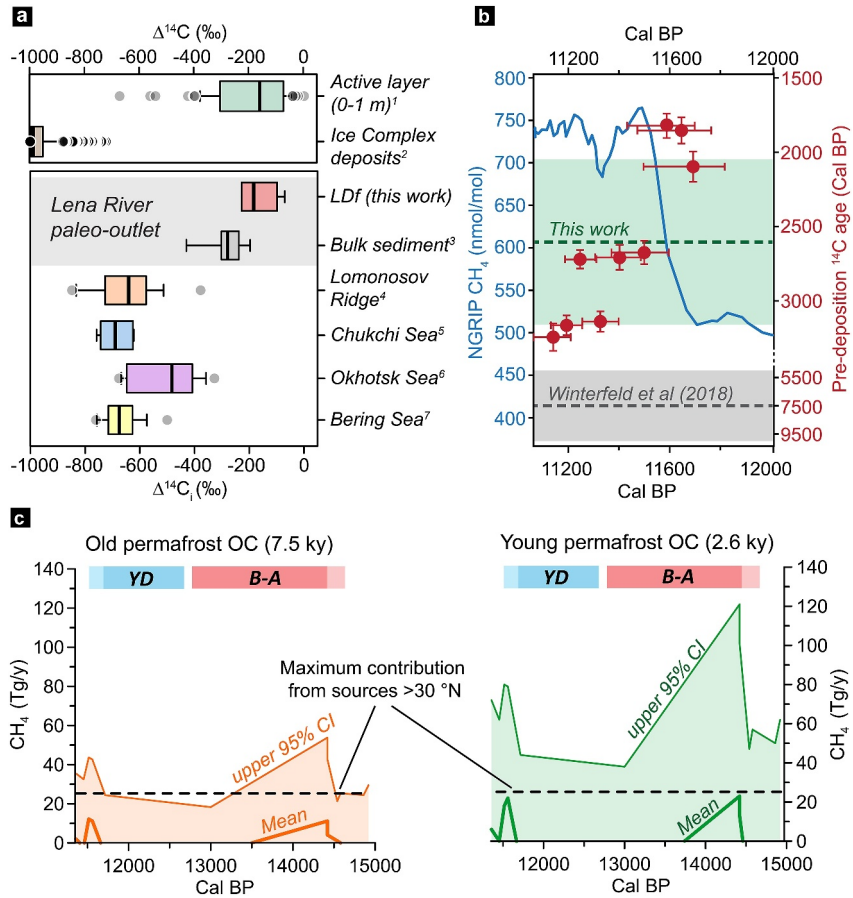

Figure 3. Radiocarbon (^{14}C) fingerprint and age of organic matter from Arctic sediments and potential methane (CH_4) emissions from terrestrial material remobilized from late deglacial permafrost systems. (a) Comparison between ^{14}C fingerprint of bulk organic carbon (OC) from modern Arctic permafrost systems (above; 1: Wild et al., 2019, 2: Martens et al., 2022), and organic matter from marine sediments deposited during Termination 1 (T1; below). Organic matter includes OC from the low density fraction (LDf; this work), bulk sediment OC (3: Tesi, Muschitiello, et al., 2016, 4: Martens et al., 2020, 5: Martens et al., 2019), and wax lipids (6: Winterfeld et al., 2018, 7: Meyer et al., 2019). Note that the end members from Wild et al. (2019) include only data from the active layer and Siberian non-permafrost surface soils, while we discarded data from the organic layer and litter that are dominated by organic matter enriched in ^{14}C after nuclear weapon tests in the contemporary system, to increase comparability with samples from T1. Note that $\Delta^{14}C$ values at deposition ($\Delta^{14}C_i$) are reported for samples from marine sediments and that the values from wax lipids (6, 7) were back calculated according to Equation 4 using published pre-depositional ^{14}C ages (long chain *n*-alkanes older than 15 ka BP where excluded due to petrogenic C contamination; cf. Meyer et al., 2019). Box plot: the thick line is the median, the edges and whiskers are 25%–75% and 10%–90% percentiles, respectively; outliers are indicated by gray dots. (b) Age of permafrost OC remobilized in the Siberian hinterland across the Younger Dryas (YD)-Preboreal transition (red dots are late deglacial samples from this study) plotted against the concentration of atmospheric CH_4 from North Greenland Ice Core Project (NGRIP, blue line; Baumgartner et al., 2012). The gray and green dashed lines show the average age assumed by Dyonisius et al. (2020; derived from Winterfeld et al., 2018) and obtained in this work, respectively; shaded areas indicate age errors. Note the scale change on the right *Y*-axis. Error bars indicate 1σ (vertical) and 2σ (horizontal). (c) Methane emissions from old (left; Dyonisius et al., 2020) and young (right; this work) permafrost OC during the late phase of T1 (positive values for mean and upper 95% confidence interval, CI, from Table 2). The dashed line is the maximum contribution from northern extratropical (>30°N) sources proposed by Riddell-Young et al. (2023). The red and light blue rectangles indicate the Bølling-Allerød (B-A) interstadial and YD stadial, respectively, with shaded colors marking abrupt atmospheric CH_4 rise events. Cal BP: calibrated years Before Present; Tg = 10^{12} g.

predominantly from Ice Complex deposits remobilized through thermokarst processes and coastal erosion (Martens et al., 2019, 2020). Average contribution from active layer OC accounted only for 17 times less than OC from Ice Complex deposits at about 15 ka BP (Martens et al., 2020), but increased to four-six times less after 13 to 10 ka BP (Martens et al., 2019, 2020), in line with the large remobilization reported from our coring site (Tesi, Muschitiello, et al., 2016).

Leaf wax lipids, common tracers of terrOM input into aquatic environments (e.g., Inglis et al., 2022), indicate coeval increasing fluxes of terrestrial OC from easternmost Siberia and Beringia to the northernmost Pacific Ocean (Meyer et al., 2019; Winterfeld et al., 2018). Moderately to strongly ^{14}C-depleted wax lipids (Figure 3a) reached the margins of the Sea of Okhotsk and the Bering Sea between 9 and 15 ka BP (Figure 1). Wax lipids derived from coastal erosion of Ice Complex deposits eroded along the coast and within the easternmost Siberia and Beringia hinterlands, with contributions from permafrost soils that were experiencing gradual to abrupt thaw (Meyer et al., 2019; Winterfeld et al., 2018).

Insights from our and previous studies collectively suggest heterogeneity in both the type of OC remobilized and release dynamics for late deglacial permafrost systems, and remark that remobilization of relatively young permafrost OC was widespread beside old permafrost OC. However, several factors can blur this complex scenario. First, the positions of the study sites are critical. All sites east of PC23 were located further away from the paleo-outlets of major Arctic rivers and/or at a greater distance from shore when sediments were deposited (Figure 1). In the modern Arctic, the relative contribution of OC from Ice Complex deposits (old and refractory) becomes overall more important compared to younger OC from topsoil and the active layer moving away from the main Arctic river outflows and offshore (Bröder et al., 2016, 2019; Matsubara et al., 2022; Vonk et al., 2012). Second, different proxies for terrOM remobilization can trace specific fractions of the heterogeneous permafrost OC pool. In detail, wax lipids carry a signal generally biased toward the old (deep) and most refractory OC part mobilized through collapse of coastal bluffs or deep thermokarst erosion (Feng et al., 2013, 2015; Gustafsson et al., 2011) and account for a small fraction of the total permafrost OC pool. Furthermore, wax lipids are more recalcitrant than most terrOM components (Bröder et al., 2018; Matsubara et al., 2022) and preferably bound to the fine mineral fraction. This promotes long residence times in soils (900–4,400 years; cf., Kusch et al., 2010) and long-range transport over the continental margin (Bröder et al., 2018; Tesi, Semiletov, et al., 2016). These features concur to increase the residence time of wax lipids prior to final deposition, thus making their ^{14}C signature less representative for $^{14}CH_4$ emissions from permafrost. Overlooking these factors may lead to underestimating the complexities of past permafrost systems, thus providing a partial view of their response to climate change.

In contrast to those sites, the PC23 study site faced the Lena River paleo-outflow receiving terrOM directly from a vast inland permafrost domain. Owing to their hydrodynamic properties, plant debris were rapidly buried into sediments, providing nearly pristine information on permafrost OC released from the Lena catchment, including OC from the shallow sub-surface of thawing permafrost soils. Additionally, plant debris delivered by Arctic rivers to continental shelves carries a signal that integrates large-scale dynamics of permafrost OC destabilization from inland domains (e.g., Guo et al., 2007; Wild et al., 2019; X. Zhang et al., 2017) and account for a much larger fraction of the total permafrost OC pool compared to wax lipids. Together, these factors concur to offer a rather unique perspective reflecting more directly the dynamics and type of terrestrial OC remobilized from a vast inland permafrost domain.

Integrating information from multiple study sites highlights the heterogeneity in terrestrial OC remobilized from late deglacial permafrost systems. The remobilization of a heterogeneous OC pool interacting with the surface water cycle implies emission of GHGs of a similarly broad spectrum of ^{14}C ages to the atmosphere. Overlooking these complexities may bias estimates of C exchange between Arctic permafrost systems and the atmosphere.

3.3. Deglacial Methane Emissions From a "Young" Permafrost OC Perspective

The release of CH_4 at the site of thaw following the reactivation of dormant permafrost OC might have induced a positive feedback to climate change during T1 (Köhler et al., 2014; Winterfeld et al., 2018). A recent study modeled CH_4 emissions from old permafrost OC assuming that all CH_4 had the same ^{14}C fingerprint as recalcitrant terrestrial leaf wax biomarkers mobilized throughout T1 in the eastern Arctic (Sea of Okhotsk; Dyonisius et al., 2020). According to the pre-depositional ^{14}C age of these old molecular fossils (Figure 3b; on average 7,500 ± 2,500 years; age calculated by Dyonisius et al. (2020) and derived from Winterfeld et al., 2018), the authors suggested small contributions of old permafrost OC to the deglacial CH_4 budget, representing a scarce positive feedback to past (and possibly future) climate change (Dyonisius et al., 2020). However, this scenario does not accurately reflect the heterogeneous composition of organic matter and the complexities of the late deglacial permafrost systems illustrated above. In fact, wax lipids selectively trace old permafrost OC through deep thermal erosion and coastal collapse (Feng et al., 2013, 2015; Gustafsson et al., 2011), a bias that is

accentuated by the offshore location of the study site. The approach adopted in this work—focusing on plant detritus in a receptor setting dominated by the Lena River and integrating extensive regions—provides a more representative signal closely reflecting the dynamics and type of permafrost OC released from a vast inland area.

Throughout our study, we highlighted the complexities of late deglacial permafrost systems and showed that in addition to several thousand years old organic matter, relatively young OC was remobilized from hinterland processes during the latest phase of the climate transition. Aiming to assess the potential impact of different carbon sources, including young permafrost OC, we applied the model from Dyonisius et al. (2020), setting the ^{14}C activity of CH_4 from this source to be equal to the average pre-depositional ^{14}C age found for plant debris intercepted at the Lena River paleo-outflow. It is important to acknowledge that the model proposed by Dyonisius et al. (2020) works best to estimate emissions from old OCs. For organic matter up to a few thousand years old, the uncertainty of CH_4 emissions increases with decreasing age of the end member (e.g., Brosius et al., 2023) due to analytical limits for $\Delta^{14}CH_4$ measurements from ice cores (Dyonisius et al., 2020; Petrenko et al., 2017). Furthermore, the same analytical limits make it virtually impossible to discriminate relatively young permafrost OC from other sources showing analogous ^{14}C fingerprint, such as OC from tropical wetlands. Considering these limits, the new estimates show how a relatively young (~2,600 years; Figure 3b) permafrost OC end-member could double the top-down constraints allowed for permafrost-derived CH_4 emissions during the late deglacial phase compared to an old end-member (7,500 ± 2,500 years; Table 2; Figure 3c), passing from a maximum of 53 Tg CH_4/yr (Dyonisius et al., 2020) to 121 Tg CH_4/yr at the end of the Oldest Dryas-Bølling transition. We remark that both these quantitative estimates are highly uncertain (cf. Supplementary Text 4.3 from Dyonisius et al., 2020). In fact, the implicit assumption that all CH_4 with a relatively young ^{14}C fingerprint is derived from permafrost OC with no emissions from other sources is most certainly untrue (cf. Supplementary Text 4.3 from Dyonisius et al. (2020) for CH_4 emissions from old permafrost OC).

The aspects outlined above make the quantification extremely challenging for permafrost OC and particularly for the younger fraction using $^{14}CH_4$-based top-down constraints alone, as reflected by the large errors (95% confidence interval, CI) associated to our and previous estimates (Table 2). Additional constraint on permafrost contribution to the deglacial CH_4 rise may be provided by studies investigating differences in the concentration of CH_4 trapped in Arctic and Antarctic ice cores (e.g., Baumgartner et al., 2012; Riddell-Young et al., 2023). Recent estimates suggest that northern extratropical (>30°N) sources, namely wetlands and/or degrading permafrost, played a secondary role in deglacial CH_4 variability (Riddell-Young et al., 2023). Methane emissions from those sources started rising at about 16 ka BP contributing at most 25 Tg CH_4/yr before 11.7 ka BP (Riddell-Young et al., 2023). Comparison with top-down estimates shows that average CH_4 emissions are in the same order of magnitude, but maximum allowable contributions (95% CI) from young (and in part also old) permafrost OC exceed the interpolar constraint, with large differences during abrupt climate transitions (Figure 3c). Such differences with top-down estimates suggest caution on maximum contributions allowed from permafrost, which are affected by the limits outlined above and therefore may be overestimated. However, while studies based on CH_4 interpolar concentration differences provide good constraints on millennial scales, they struggle to resolve abrupt and short lived (annual to decadal) changes of atmospheric CH_4 concentration (cf. Riddell-Young et al., 2023). Although no strong constraint can be provided, this leaves open the possibility of a larger involvement of permafrost OC in the deglacial CH_4 budget, especially when its younger fraction is considered.

Here, we investigate the contribution of young (about 2.6 ky old) OC remobilized from past permafrost systems to the deglacial CH_4 rise. Although we cannot provide strong constraints, our results suggest that remobilization of relatively young terrestrial OC from inland permafrost systems possibly exerted a stronger positive feedback to deglacial climate change through CH_4 emissions.

3.4. "Young" Permafrost OC and Methane Emissions

The impact that CH_4 emissions from thawing permafrost had on climate change throughout T1 is still debated (Jones et al., 2023 and references therein). Some studies have shown through different approaches that old permafrost OC exerted only limited forcing on past climate change through CH_4 fluxes to the atmosphere (Brosius et al., 2023; Dyonisius et al., 2020; Petrenko et al., 2017; Walter Anthony et al., 2014). However, old permafrost OC represents only part of the highly heterogeneous total OC pool remobilized throughout the deglaciation such as across the extensive Lena River watershed.

In this study, we show that accounting for the largely unexplored few millennia old fraction of the permafrost OC pool may require revising (increasing) contributions to deglacial CH_4 emissions and hence the positive feedback to warming. In fact, several lines of evidence may support greater CH_4 emissions from permafrost than previously thought. First, multiple reports of OC remobilization from the active layer were found throughout T1 (see Section 3.2). Incubation experiments demonstrated that active layer OC has a great potential to be emitted as CH_4 at site (four times than OC from permafrost; Treat et al., 2015), particularly when it derives from highly decomposable organic remains of graminoids (Olefeldt et al., 2013; Treat et al., 2015). It is likely that the reactivation of relatively young and scarcely decomposed remains of tundra-steppe flora due to rapid active layer thickening in response to fast warming events during T1 boosted CH_4 emissions to the atmosphere. Second, the Arctic permafrost became progressively wetter and warmer (MacDonald et al., 2006; Walter et al., 2007). Wet areas expanded fast in the second half of T1 (Brosius et al., 2021; Nichols & Peteet, 2019; Treat et al., 2019, 2021), with widespread ponding indicating still largely inactive deep permafrost conduits. Rapid thickening of the active layer after abrupt warming combined with poor draining conditions might have promoted widespread water-saturation and anoxia in formerly dry soils from Arctic tundra landscapes and particularly in lowlands. Here, it is plausible that CH_4 emissions were favored over CO_2 emissions due to anaerobic decomposition of newly available terrOM after active layer deepening. Methane fluxes likely increased areally in the summer season, when methanogenesis is favored by higher temperatures (Tveit et al., 2015). These fluxes would have been deleterious for the deglacial climate by adding previously sequestered carbon to CH_4 emissions from the recycling of contemporaneous OC in growing wetlands (Treat et al., 2019, 2021). Discontinuous water-logged conditions possibly attenuated CH_4 fluxes from the active layer through CH_4 oxidation (Dean et al., 2018; and references therein), which is also promoted in a warmer active layer (Yergeau et al., 2010). However, complete methanogenesis stoppage is unlikely (e.g., van Winden et al., 2012), potentially supporting increased CH_4 fluxes from a thicker active layer when favorable conditions developed. Third, a longer "zero curtain" period (*sensu* Zona et al., 2016) might have characterized the cold season (fall to spring) during past abrupt warming events. In the cold season, freezing back of the active layer from the top and the bottom lowers CH_4 oxidation causing net emission rates from the still unfrozen active layer in between to increase (Zona et al., 2016). In the modern Arctic, cold season emissions may account for more than 50% of the annual CH_4 flux, reaching the highest rates in non-inundated upland tundra (Zona et al., 2016). Analogously, a thicker active layer promoted by rapid warming events during T1 might have elongated the "zero curtain" period leading to higher CH_4 fluxes to the atmosphere during the cold season from areas of the non-inundated upland tundra-steppe paleo-domain. Fourth, evidence from the modern terrestrial permafrost systems revealed that contemporaneous to few millennia old terrOM has the greatest potential to fuel CH_4 emissions (Cooper et al., 2017; Elder et al., 2018; Estop-Aragonés et al., 2018). This is supported by observations from sites affected by deep thermokarst processes, where in several cases the emitted CH_4 shows a contemporaneous to few thousand years ^{14}C age rather than being tens of thousands years old as OC reactivated from deep permafrost layers (Estop-Aragonés et al., 2020). The release of previously unavailable relatively young permafrost OC following rapid active layer thickening might therefore support enhanced fluxes of similarly young CH_4 to the atmosphere, boosting incipient emissions from newly formed wetlands (Nichols & Peteet, 2019; Treat et al., 2021) and thermokarst lakes (Brosius et al., 2021, 2023; Walter Anthony et al., 2014; Walter et al., 2007). Lastly, it is noticeable that both at the end of the Oldest Dryas-Bølling transition and during the YD-PB transition the model returns mean CH_4 emissions (13–23 Tg CH_4/yr and 18–22 Tg CH_4/yr, respectively; in italics in Table 2, Figure 3c) that are in the same order of magnitude of year-round estimates from the modern circumpolar Arctic tundra domain undergoing active layer thickening (23 ± 8 Tg CH_4/yr; Zona et al., 2016). Despite large uncertainties, this would agree with stronger year-round CH_4 emissions from deglacial permafrost systems, which would be in line with the greater areal extent of the tundra steppe-domain during T1 (Ashastina et al., 2017; Baumer et al., 2021). This may suggest that CH_4 fluxes from hinterland permafrost areas undergoing rapid active layer thickening in response to fast warming during abrupt climate transitions contributed substantially to emissions from northern extratropical sources.

Examining evidence from the modern and ancient Arctic and integrating the so-far overlooked permafrost OC fraction up to a few thousand years old, we propose that the contribution of permafrost OC to the deglacial CH_4 budget was stronger than hypothesized so far. The complexities of permafrost systems require careful evaluation and recommend caution when addressing the impact from this OC source on past (and possibly future) climate change.

4. Conclusions

This work explores the release of permafrost OC throughout Termination 1 (ca. 11.7–18 ka BP), highlighting the complexities of permafrost systems and their potential impact as forcing factors for climate change through emissions of methane to the atmosphere. Specifically, we focus on the YD-Preboreal transition (ca. 11.6 ka BP) when the concentration of atmospheric methane increased sharply. The results show that the Siberian permafrost domain reacted to the rapid warming event through a redistribution of carbon in the major pools involving the relatively young (about 2,600 yr) terrestrial organic matter stored in active layer soils. The release of relatively young terrestrial organic matter to the Arctic Ocean during the YD-PB transition and to some extent during previous rapid warming events likely resulted in fluxes of methane with analogous age to the atmosphere from the expansive inland Arctic permafrost domain. This study stresses that missing the complexities of permafrost systems may blur the comprehension of the permafrost OC-climate feedback. In the next decades, warming is expected to trigger permafrost loss on a pan-Arctic scale (ICCI, 2023) through deepening of the active layer (IPCC, 2023; Smith et al., 2022) and abrupt thaw events (Meredith et al., 2019; Turetsky et al., 2020). In particular, widespread active layer thickening down to 1 m depth may reactivate a highly vulnerable OC pool accounting for about one third (Mishra et al., 2021) of the 1,600 Pg OC stored in permafrost soils (Hugelius et al., 2014; Tarnocai et al., 2009). These processes will release permafrost OC covering the entire age spectrum from the modern to the late Pleistocene (>50 ky old), resulting in permanent (on a human timescale) emissions of GHGs to the atmosphere (ICCI, 2023). Implementing the complexities of permafrost systems involving more components of this highly heterogeneous OC pool (including the most vulnerable few millennia old fraction) will be crucial to improve estimates and modeling of both past and future fluxes of GHGs from the Arctic in response to climate warming.

Data Availability Statement

All data supporting this publication are available in Supporting Information S1 and freely accessible (CC-BY: Creative Commons Attribution 4.0 International) at the PANGAEA database (https://doi.org/10.1594/PANGAEA.972409 and https://doi.org/10.1594/PANGAEA.972412, Sabino et al., 2024a, 2024b). We refer to M. N. Dyonisius to request for the MATLAB code used for modeling methane emissions.

Acknowledgments

We thank all collaboration partners who over the years have been involved in the sampling and analysis that contributed to the current data set. The SWERUS-C3 program was supported by the Knut and Alice Wallenberg Foundation (KAW contract 2011.0027 to ÖG). This work was also supported by the European Research Council (ERC Advanced Grant CC-TOP 695331 to ÖG), the Swedish Research Council (Grant 2017-01601 to ÖG), the Russian Science Foundation (Grant 21-77-30001 to IS), the Russian Ministry of Science and higher Education (Grants 0211-2021-0010 and 12102100057-4 to Pacific Oceanological Institute FEB RAS). BW additionally acknowledges Formas Grant 2021-01750. This work has been principally funded and conducted in the framework of the Joint Research Center ENI-CNR—"Aldo Pontremoli" within the ENI-CNR Joint Research Agreement WP1 "Impatto delle emissioni in atmosfera sulla criosfera e sul cambiamento climatico nell'Artico". We further thank F. Corticelli and L. Capotondi for capturing SEM digital microphotos; F. Bozzeda and G. Pappacogli for assistance in the modelling part; M. N. Dyonisius for sharing and giving insights into the scripts to run the emission model. We thank M. N. Dyonisius and an anonymous reviewer for their insightful comments that helped improve the study. Open access publishing facilitated by Consiglio Nazionale delle Ricerche, as part of the Wiley - CRUI-CARE agreement.

References

Amon, R. M. W., Rinehart, A. J., Duan, S., Louchouarn, P., Prokushkin, A., Guggenberger, G., et al. (2012). Dissolved organic matter sources in large Arctic rivers. *Geochimica et Cosmochimica Acta*, *94*, 217–237. https://doi.org/10.1016/j.gca.2012.07.015

Andreev, A. A., Schirrmeister, L., Tarasov, P. E., Ganopolski, A., Brovkin, V., Siegert, C., et al. (2011). Vegetation and climate history in the Laptev Sea region (Arctic Siberia) during Late Quaternary inferred from pollen records. *Quaternary Science Reviews*, *30*(17–18), 2182–2199. https://doi.org/10.1016/j.quascirev.2010.12.026

Andresen, C. G., Lawrence, D. M., Wilson, C. J., David McGuire, A., Koven, C., Schaefer, K., et al. (2020). Soil moisture and hydrology projections of the permafrost region-a model intercomparison. *The Cryosphere*, *14*(2), 445–459. https://doi.org/10.5194/tc-14-445-2020

Ashastina, K., Kuzmina, S., Rudaya, N., Troeva, E., Schoch, W. H., Römermann, C., et al. (2018). Woodlands and steppes: Pleistocene vegetation in Yakutia's most continental part recorded in the Batagay permafrost sequence. *Quaternary Science Reviews*, *196*, 38–61. https://doi.org/10.1016/j.quascirev.2018.07.032

Ashastina, K., Schirrmeister, L., Fuchs, M., & Kienast, F. (2017). Palaeoclimate characteristics in interior Siberia of MIS 6-2: First insights from the Batagay permafrost mega-thaw slump in the Yana Highlands. *Climate of the Past*, *13*(7), 795–818. https://doi.org/10.5194/cp-13-795-2017

Bauch, H. A., & Kassens, H. (2005). Arctic Siberian shelf environments—An introduction. *Global and Planetary Change*, *48*(1–3), 1–8. https://doi.org/10.1016/j.gloplacha.2004.12.003

Bauch, H. A., Mueller-Lupp, T., Taldenkova, E., Spielhagen, R. F., Kassens, H., Grootes, P. M., et al. (2001). Chronology of the holocene transgression at the north siberian margin. *Global and Planetary Change*, *31*(1–4), 125–139. https://doi.org/10.1016/S0921-8181(01)00116-3

Baumer, M. M., Wagner, B., Meyer, H., Leicher, N., Lenz, M., Fedorov, G., et al. (2021). Climatic and environmental changes in the Yana Highlands of north-eastern Siberia over the last 57 ky, Lake Emanda. *Boreas*, *50*(1), 114–133. https://doi.org/10.1111/bor.12476

Baumgartner, M., Schilt, A., Eicher, O., Schmitt, J., Schwander, J., Spahni, R., et al. (2012). *NOAA/WDS paleoclimatology—NGRIP and EDML ice core 32–11 kyr BP methane data. Subset: NGRIP2012CH4*. NOAA National Centers for Environmental Information. https://doi.org/10.25921/7gzt-c915

Benner, R., Weliky, K., & Hedges, J. I. (1990). Early diagenesis of mangrove leaves in a tropical estuary: Molecular-level analyses of neutral sugars and lignin-derived phenols. *Geochimica et Cosmochimica Acta*, *54*(7), 1991–2001. https://doi.org/10.1016/0016-7037(90)90267-O

Bergamaschi, B. A., Tsamakis, E., Keil, R. G., Eglinton, T. I., Montluçon, D. B., & Hedges, J. I. (1997). The effect of grain size and surface area on organic matter, lignin and carbohydrate concentration, and molecular compositions in Peru Margin sediments. *Geochimica et Cosmochimica Acta*, *61*(6), 1247–1260. https://doi.org/10.1016/S0016-7037(96)00394-8

Biskaborn, B. K., Subetto, D. A., Savelieva, L. A., Vakhrameeva, P. S., Hansche, A., Herzschuh, U., et al. (2016). Late Quaternary vegetation and lake system dynamics in north-eastern Siberia: Implications for seasonal climate variability. *Quaternary Science Reviews*, *147*, 406–421. https://doi.org/10.1016/j.quascirev.2015.08.014

Bröder, L., Andersson, A., Tesi, T., Semiletov, I., & Gustafsson, Ö. (2019). Quantifying degradative loss of terrigenous organic carbon in surface sediments across the Laptev and East Siberian sea. *Global Biogeochemical Cycles*, *33*(1), 85–99. https://doi.org/10.1029/2018GB005967

Bröder, L., Keskitalo, K., Zolkos, S., Shakil, S., Tank, S. E., Kokelj, S. V., et al. (2021). Preferential export of permafrost-derived organic matter as retrogressive thaw slumping intensifies. *Environmental Research Letters*, *16*(5), 054059. https://doi.org/10.1088/1748-9326/abee4b

Bröder, L., Tesi, T., Andersson, A., Semiletov, I., & Gustafsson, Ö. (2018). Bounding cross-shelf transport time and degradation in Siberian-Arctic land-ocean carbon transfer. *Nature Communications*, *9*(1), 1–8. https://doi.org/10.1038/s41467-018-03192-1

Bröder, L., Tesi, T., Salvadó, J. A., Semiletov, I. P., Dudarev, O. V., & Gustafsson, O. (2016). Fate of terrigenous organic matter across the Laptev Sea from the mouth of the Lena River to the deep sea of the Arctic interior. *Biogeosciences*, *13*(17), 5003–5019. https://doi.org/10.5194/bg-13-5003-2016

Bronk Ramsey, C. (2008). Deposition models for chronological records. *Quaternary Science Reviews*, *27*(1–2), 42–60. https://doi.org/10.1016/j.quascirev.2007.01.019

Bronk Ramsey, C. (2009). Bayesian analysis of radiocarbon dates. *Radiocarbon*, *51*(1), 337–360. https://doi.org/10.1017/s0033822200033865

Brosius, L. S., Anthony, K. M. W., Treat, C. C., Lenz, J., Jones, M. C., Bret-Harte, M. S., & Grosse, G. (2021). Spatiotemporal patterns of northern lake formation since the Last Glacial Maximum. *Quaternary Science Reviews*, *253*, 106773. https://doi.org/10.1016/j.quascirev.2020.106773

Brosius, L. S., Walter Anthony, K. M., Treat, C. C., Jones, M. C., Dyonisius, M., & Grosse, G. (2023). Panarctic lakes exerted a small positive feedback on early Holocene warming due to deglacial release of methane. *Communications Earth and Environment*, *4*(1), 1–11. https://doi.org/10.1038/s43247-023-00930-2

Brown, J., Ferrians, O. J., Jr., Heginbottom, J. A., & Melinkov, E. S. (1997). *Circum-Arctic map of permafrost and ground-ice conditions*. US Geological Survey (Volume Circum-Pacific). https://doi.org/10.3133/cp45

Buizert, C., Adrian, B., Ahn, J., Albert, M., Alley, R. B., Baggenstos, D., et al. (2015). Precise interpolar phasing of abrupt climate change during the last ice age. *Nature*, *520*(7549), 661–665. https://doi.org/10.1038/nature14401

Cao, M., Hefter, J., Tiedemann, R., Lembke-Jene, L., Meyer, V. D., & Mollenhauer, G. (2023). Deglacial records of terrigenous organic matter accumulation off the Yukon and Amur rivers based on lignin phenols and long-chain n-alkanes. *Climate of the Past*, *19*(1), 159–178. https://doi.org/10.5194/cp-19-159-2023

Chevychelov, A. P., & Bosikov, N. P. (2010). Natural conditions. In E. Troeva, A. Isaev, M. Cherosov, & N. Karpov (Eds.), *The far North. Plant and vegetation* (Vol. 3, pp. 390–423). Springer. https://doi.org/10.1007/978-90-481-3774-9_1

Ciais, P., Tagliabue, A., Cuntz, M., Bopp, L., Scholze, M., Hoffmann, G., et al. (2012). Large inert carbon pool in the terrestrial biosphere during the Last Glacial Maximum. *Nature Geoscience*, *5*(1), 74–79. https://doi.org/10.1038/ngeo1324

Cooper, M. D. A., Estop-Aragonés, C., Fisher, J. P., Thierry, A., Garnett, M. H., Charman, D. J., et al. (2017). Limited contribution of permafrost carbon to methane release from thawing peatlands. *Nature Climate Change*, *7*(7), 507–511. https://doi.org/10.1038/nclimate3328

Dao, T. T., Mikutta, R., Sauheitl, L., Gentsch, N., Shibistova, O., Wild, B., et al. (2022). Lignin preservation and microbial carbohydrate metabolism in permafrost soils. *Journal of Geophysical Research: Biogeosciences*, *127*(1), e2020JG006181. https://doi.org/10.1029/2020JG006181

Dao, T. T., Mikutta, R., Wild, B., Sauheitl, L., Gentsch, N., Shibistova, O., et al. (2023). How temperature and aridity drive lignin decomposition along a latitudinal transect in Western Siberia. *European Journal of Soil Science*, *74*(5), 1–16. https://doi.org/10.1111/ejss.13408

Dean, J. F., Middelburg, J. J., Röckmann, T., Aerts, R., Blauw, L. G., Egger, M., et al. (2018). Methane feedbacks to the global climate system in a warmer world. *Reviews of Geophysics*, *56*(1), 207–250. https://doi.org/10.1002/2017RG000559

Denton, G. H., Anderson, R. F., Toggweiler, J. R., Edwards, R. L., Schaefer, J. M., & Putnam, A. E. (2010). The last glacial termination. *Science*, *328*(5986), 1652–1656. https://doi.org/10.1126/science.1184119

Dickens, A. F., Baldock, J., Kenna, T. C., & Eglinton, T. I. (2011). A depositional history of particulate organic carbon in a floodplain lake from the lower Ob' River, Siberia. *Geochimica et Cosmochimica Acta*, *75*(17), 4796–4815. https://doi.org/10.1016/j.gca.2011.05.032

Dickens, A. F., Gélinas, Y., & Hedges, J. I. (2004). Physical separation of combustion and rock sources of graphitic black carbon in sediments. *Marine Chemistry*, *92*(1–4), 215–223. https://doi.org/10.1016/j.marchem.2004.06.027

Dyonisius, M. N., Petrenko, V. V., Smith, A. M., Hua, Q., Yang, B., Schmitt, J., et al. (2020). Old carbon reservoirs were not important in the deglacial methane budget. *Science*, *367*(6480), 907–910. https://doi.org/10.1126/science.aax0504

Elder, C. D., Xu, X., Walker, J., Schnell, J. L., Hinkel, K. M., Townsend-Small, A., et al. (2018). Greenhouse gas emissions from diverse Arctic Alaskan lakes are dominated by young carbon. *Nature Climate Change*, *8*(2), 166–171. https://doi.org/10.1038/s41558-017-0066-9

Estop-Aragonés, C., Cooper, M. D. A., Fisher, J. P., Thierry, A., Garnett, M. H., Charman, D. J., et al. (2018). Limited release of previously-frozen C and increased new peat formation after thaw in permafrost peatlands. *Soil Biology and Biochemistry*, *118*(August 2017), 115–129. https://doi.org/10.1016/j.soilbio.2017.12.010

Estop-Aragonés, C., Olefeldt, D., Abbott, B. W., Chanton, J. P., Czimczik, C. I., Dean, J. F., et al. (2020). Assessing the potential for mobilization of old soil carbon after permafrost thaw: A synthesis of ^{14}C measurements from the northern permafrost region. *Global Biogeochemical Cycles*, *34*(9), 26. https://doi.org/10.1029/2020GB006672

Feng, X., Gustafsson, Ö., Holmes, R. M., Vonk, J. E., Van Dongen, B. E., Semiletov, I. P., et al. (2015). Multimolecular tracers of terrestrial carbon transfer across the pan-arctic: ^{14}C characteristics of sedimentary carbon components and their environmental controls. *Global Biogeochemical Cycles*, *29*(11), 1855–1873. https://doi.org/10.1002/2015GB005204

Feng, X., Vonk, J. E., Van Dongen, B. E., Gustafsson, Ö., Semiletov, I. P., Dudarev, O. V., et al. (2013). Differential mobilization of terrestrial carbon pools in Eurasian Arctic river basins. *Proceedings of the National Academy of Sciences of the United States of America*, *110*(35), 14168–14173. https://doi.org/10.1073/pnas.1307031110

Gentsch, N., Wild, B., Mikutta, R., Čapek, P., Diáková, K., Schrumpf, M., et al. (2018). Temperature response of permafrost soil carbon is attenuated by mineral protection. *Global Change Biology*, *24*(8), 3401–3415. https://doi.org/10.1111/gcb.14316

Goñi, M. A., & Hedges, J. I. (1995). Sources and reactivities of marine-derived organic matter in coastal sediments as determined by alkaline CuO oxidation. *Geochimica et Cosmochimica Acta*, *59*(14), 2965–2981. https://doi.org/10.1016/0016-7037(95)00188-3

Goñi, M. A., & Montgomery, S. (2000). Alkaline CuO oxidation with a microwave digestion system: Lignin analyses of geochemical samples. *Analytical Chemistry*, *72*(14), 3116–3121. https://doi.org/10.1021/ac991316w

Grosse, G., Harden, J., Turetsky, M., McGuire, A. D., Camill, P., Tarnocai, C., et al. (2011). Vulnerability of high-latitude soil organic carbon in North America to disturbance. *Journal of Geophysical Research*, *116*(3), G00K06. https://doi.org/10.1029/2010JG001507

Guo, L., Ping, C. L., & Macdonald, R. W. (2007). Mobilization pathways of organic carbon from permafrost to arctic rivers in a changing climate. *Geophysical Research Letters*, *34*(13), 1–5. https://doi.org/10.1029/2007GL030689

Guo, L., Semiletov, I., Gustafsson, Ö., Ingri, J., Andersson, P., Dudarev, O., & White, D. (2004). Characterization of Siberian Arctic coastal sediments: Implications for terrestrial organic carbon export. *Global Biogeochemical Cycles*, *18*(1), GB1036. https://doi.org/10.1029/2003gb002087

Gustafsson, Ö., Van Dongen, B. E., Vonk, J. E., Dudarev, O. V., & Semiletov, I. P. (2011). Widespread release of old carbon across the Siberian Arctic echoed by its large rivers. *Biogeosciences*, *8*(6), 1737–1743. https://doi.org/10.5194/bg-8-1737-2011

Heaton, T. J., Butzin, M., Bard, E., Bronk Ramsey, C., Hughen, K. A., Kohler, P., & Reimer, P. J. (2023). Marine radiocarbon calibration in polar regions: A simple approximate approach using marine20. *Radiocarbon*, *65*(4), 848–875. https://doi.org/10.1017/RDC.2023.42

Heaton, T. J., Köhler, P., Butzin, M., Bard, E., Reimer, R. W., Austin, W. E. N., et al. (2020). Marine20—The marine radiocarbon age calibration curve (0–55,000 cal BP). *Radiocarbon*, *62*(4), 779–820. https://doi.org/10.1017/RDC.2020.68

Hedges, J. I., Keil, R. G., & Benner, R. (1997). What happens to terrestrial organic matter in the ocean? *Organic Geochemistry*, *27*(5–6), 195–212. https://doi.org/10.1016/S0146-6380(97)00066-1

Hedges, J. I., & Mann, D. C. (1979). The characterization of plant tissues by their lignin oxidation products. *Geochimica et Cosmochimica Acta*, *43*(11), 1803–1807. https://doi.org/10.1016/0016-7037(79)90028-0

Hedges, J. I., & Prahl, F. G. (1993). Early diagenesis: Consequences for applications of molecular biomarkers. In M. H. Engel, S. A. Macko, & D. S. Jones (Eds.), *Organic geochemistry, principles and applications* (pp. 237–253). Plenum Press. https://doi.org/10.1007/978-1-4615-2890-6_11

Hua, Q., Barbetti, M., & Rakowski, A. Z. (2013). Atmospheric radiocarbon for the period 1950–2010. *Radiocarbon*, *55*(4), 2059–2072. https://doi.org/10.2458/azu_js_rc.v55i2.16177

Hugelius, G., Strauss, J., Zubrzycki, S., Harden, J. W., Schuur, E. A. G., Ping, C. L., et al. (2014). Estimated stocks of circumpolar permafrost carbon with quantified uncertainty ranges and identified data gaps. *Biogeosciences*, *11*(23), 6573–6593. https://doi.org/10.5194/bg-11-6573-2014

ICCI. (2023). State of the cryosphere 2023—Two degrees is too high. In *International cryosphere climate initiative (ICCI), Stockholm, Sweden*.

Inglis, G. N., Bhattacharya, T., Hemingway, J. D., Hollingsworth, E. H., Feakins, S. J., & Tierney, J. E. (2022). Biomarker approaches for reconstructing terrestrial environmental change. *Annual Review of Earth and Planetary Sciences*, *50*(February), 369–394. https://doi.org/10.1146/annurev-earth-032320-095943

Intergovernmental Panel on Climate Change (IPCC). (2023). Ocean, cryosphere and sea level change. In *Climate change 2021 – The physical science basis* (pp. 1211–1362). Cambridge University Press. https://doi.org/10.1017/9781009157896.011

Jakobsson, M., Grantz, A., Kristoffersen, Y., & Macnab, R. (2004). Physiography and bathymetry of the Arctic Ocean. In R. Stein & R. W. Macdonald (Eds.), *The organic carbon cycle in the Arctic Ocean* (p. 363). Springer-Verlag.

Jones, M. C., Grosse, G., Treat, C., Turetsky, M., Anthony, K. W., & Brosius, L. (2023). Past permafrost dynamics can inform future permafrost carbon-climate feedbacks. *Communications Earth and Environment*, *4*(1), 1–13. https://doi.org/10.1038/s43247-023-00886-3

Katsuta, N., Ikeda, H., Shibata, K., Saito-Kokubu, Y., Murakami, T., Tani, Y., et al. (2018). Hydrological and climate changes in southeast Siberia over the last 33 kyr. *Global and Planetary Change*, *164*, 11–26. https://doi.org/10.1016/j.gloplacha.2018.02.012

Katsuta, N., Matsumoto, G. I., Hase, Y., Tayasu, I., Haraguchi, T. F., Tani, E., et al. (2019). Siberian permafrost thawing accelerated at the Bølling/Allerød and Preboreal warm periods during the last deglaciation. *Geophysical Research Letters*, *46*(23), 13961–13971. https://doi.org/10.1029/2019GL084726

Keil, R. G., Tsamakis, E., Giddings, J. C., & Hedges, J. I. (1998). Biochemical distributions (amino acids, neutral sugars, and lignin phenols) among size-classes of modern marine sediments from the Washington coast. *Geochimica et Cosmochimica Acta*, *62*(8), 1347–1364. https://doi.org/10.1016/S0016-7037(98)00080-5

Kobe, F., Leipe, C., Shchetnikov, A. A., Hoelzmann, P., Gliwa, J., Olschewski, P., et al. (2022). Not herbs and forbs alone: Pollen-based evidence for the presence of boreal trees and shrubs in Cis-Baikal (eastern Siberia) derived from the last glacial maximum sediment of lake Ochaul. *Journal of Quaternary Science*, *37*(5), 868–883. https://doi.org/10.1002/jqs.3290

Köhler, P., Knorr, G., & Bard, E. (2014). Permafrost thawing as a possible source of abrupt carbon release at the onset of the Bølling/Allerød. *Nature Communications*, *5*, 1–10. https://doi.org/10.1038/ncomms6520

Köhler, P., Nehrbass-Ahles, C., Schmitt, J., Stocker, T. F., & Fischer, H. (2017). A 156 kyr smoothed history of the atmospheric greenhouse gases CO_2, CH_4, and N_2O and their radiative forcing. *Earth System Science Data*, *9*(1), 363–387. https://doi.org/10.5194/essd-9-363-2017

Körner, C., Farquhar, G. D., & Wong, S. C. (1991). Carbon isotope discrimination by plants follows latitudinal and altitudinal trends. *Oecologia*, *88*(1), 30–40. https://doi.org/10.1007/BF00328400

Kostrova, S. S., Biskaborn, B. K., Pestryakova, L. A., Fernandoy, F., Lenz, M. M., & Meyer, H. (2021). Climate and environmental changes of the Lategacial transition and Holocene in northeastern Siberia: Evidence from diatom oxygen isotopes and assemblage composition at Lake Emanda. *Quaternary Science Reviews*, *259*, 106905. https://doi.org/10.1016/j.quascirev.2021.106905

Kristensen, D. K., Kristensen, E., Forchhammer, M. C., Michelsen, A., & Schmidt, N. M. (2011). Arctic herbivore diet can be inferred from stable carbon and nitrogen isotopes in C3 plants, faeces, and wool. *Canadian Journal of Zoology*, *89*(10), 892–899. https://doi.org/10.1139/z11-073

Kusch, S., Rethemeyer, J., Schefuß, E., & Mollenhauer, G. (2010). Controls on the age of vascular plant biomarkers in Black Sea sediments. *Geochimica et Cosmochimica Acta*, *74*(24), 7031–7047. https://doi.org/10.1016/j.gca.2010.09.005

Lindgren, A., Hugelius, G., & Kuhry, P. (2018). Extensive loss of past permafrost carbon but a net accumulation into present-day soils. *Nature*, *560*(7717), 219–222. https://doi.org/10.1038/s41586-018-0371-0

Lindgren, A., Hugelius, G., Kuhry, P., Christensen, T. R., & Vandenberghe, J. (2016). GIS-based maps and area estimates of Northern Hemisphere permafrost extent during the Last Glacial Maximum. *Permafrost and Periglacial Processes*, *27*(1), 6–16. https://doi.org/10.1002/ppp.1851

MacDonald, G. M., Beilman, D. W., Kremenetski, K. V., Sheng, Y., Smith, L. C., & Velichko, A. A. (2006). Rapid early development of circumarctic peatlands and atmospheric CH_4 and CO_2 variations. *The Holocene*, *314*(October), 285–288. https://doi.org/10.1126/science.1131722

Martens, J., Romankevich, E., Semiletov, I., Wild, B., Van Dongen, B., Vonk, J., et al. (2021). CASCADE-the circum-arctic sediment CArbon DatabasE. *Earth System Science Data*, *13*(6), 2561–2572. https://doi.org/10.5194/essd-13-2561-2021

Martens, J., Wild, B., Muschitiello, F., O'Regan, M., Jakobsson, M., Semiletov, I., et al. (2020). Remobilization of dormant carbon from Siberian-Arctic permafrost during three past warming events. *Science Advances*, *6*(42), eabb6546. https://doi.org/10.1126/sciadv.abb6546

Martens, J., Wild, B., Pearce, C., Tesi, T., Andersson, A., Bröder, L., et al. (2019). Remobilization of old permafrost carbon to Chukchi Sea sediments during the end of the last deglaciation. *Global Biogeochemical Cycles*, *33*(1), 2–14. https://doi.org/10.1029/2018GB005969

Martens, J., Wild, B., Semiletov, I., Dudarev, O. V., & Gustafsson, Ö. (2022). Circum-Arctic release of terrestrial carbon varies between regions and sources. *Nature Communications*, *13*(1), 5858. https://doi.org/10.1038/s41467-022-33541-0

Matsubara, F., Wild, B., Martens, J., Andersson, A., Wennström, R., Bröder, L., et al. (2022). Molecular-multiproxy assessment of land-derived organic matter degradation over extensive scales of the East Siberian arctic shelf seas. *Global Biogeochemical Cycles*, *36*(12), e2022GB007428. https://doi.org/10.1029/2022GB007428

McClelland, J. W., Holmes, R. M., Peterson, B. J., Raymond, P. A., Striegl, R. G., Zhulidov, A. V., et al. (2016). Particulate organic carbon and nitrogen export from major Arctic rivers. *Global Biogeochemical Cycles*, *30*(5), 629–643. https://doi.org/10.1002/2015GB005351

Meredith, M., Sommerkorn, M., Cassotta, S., Derksen, C., Ekaykin, A., Hollowed, A., et al. (2019). Polar regions. In H.-O. Pörtner, D. C. Roberts, V. Masson-Delmotte, P. Zhai, M. Tignor, E. Poloczanska, et al. (Eds.), *IPCC special report on the Ocean and cryosphere in a changing climate, chapter 3* (pp. 203–320). https://doi.org/10.1016/S1366-7017(01)00066-6

Meyer, V. D., Hefter, J., Köhler, P., Tiedemann, R., Gersonde, R., Wacker, L., & Mollenhauer, G. (2019). Permafrost-carbon mobilization in Beringia caused by deglacial meltwater runoff, sea-level rise and warming. *Environmental Research Letters*, *14*(8), 85003. https://doi.org/10.1088/1748-9326/ab2653

Mishra, U., Hugelius, G., Shelef, E., Yang, Y., Strauss, J., Lupachev, A., et al. (2021). Spatial heterogeneity and environmental predictors of permafrost region soil organic carbon stocks. *Science Advances*, *7*(9), 1–13. https://doi.org/10.1126/sciadv.aaz5236

Nichols, J. E., & Peteet, D. M. (2019). Rapid expansion of northern peatlands and doubled estimate of carbon storage. *Nature Geoscience*, *12*(11), 917–921. https://doi.org/10.1038/s41561-019-0454-z

Nieuwenhuize, J., Maas, Y. E. M., & Middelburg, J. J. (1994). Rapid analysis of organic carbon and nitrogen in particulate materials. *Marine Chemistry*, *45*(3), 217–224. https://doi.org/10.1016/0304-4203(94)90005-1

Nogarotto, A., Noormets, R., Chauhan, T., Mollenhauer, G., Hefter, J., Grotheer, H., et al. (2023). Coastal permafrost was massively eroded during the Bølling-Allerød warm period. *Communications Earth & Environment*, *4*(1), 350. https://doi.org/10.1038/s43247-023-01013-y

Olefeldt, D., Turetsky, M. R., Crill, P. M., & Mcguire, A. D. (2013). Environmental and physical controls on northern terrestrial methane emissions across permafrost zones. *Global Change Biology*, *19*(2), 589–603. https://doi.org/10.1111/gcb.12071

Opsahl, S., & Benner, R. (1995). Early diagenesis of vascular plant tissues: Lignin and cutin decomposition and biogeochemical implications. *Geochimica et Cosmochimica Acta*, *59*(23), 4889–4904. https://doi.org/10.1016/0016-7037(95)00348-7

Osman, M. B., Tierney, J. E., Zhu, J., Tardif, R., Hakim, G. J., King, J., & Poulsen, C. J. (2021). Globally resolved surface temperatures since the last glacial maximum. *Nature*, *599*(7884), 239–244. https://doi.org/10.1038/s41586-021-03984-4

Otto, A., & Simpson, M. J. (2006). Evaluation of CuO oxidation parameters for determining the source and stage of lignin degradation in soil. *Biogeochemistry*, *80*(2), 121–142. https://doi.org/10.1007/s10533-006-9014-x

Petrenko, V. V., Smith, A. M., Schaefer, H., Riedel, K., Brook, E., Baggenstos, D., et al. (2017). Minimal geological methane emissions during the Younger Dryas-Preboreal abrupt warming event. *Nature*, *548*(7668), 443–446. https://doi.org/10.1038/nature23316

Prahl, F. G., Ertel, J. R., Goni, M. A., Sparrow, M. A., & Eversmeyer, B. (1994). Terrestrial organic carbon contributions to sediments on the Washington margin. *Geochimica et Cosmochimica Acta*, *58*(14), 3035–3048. https://doi.org/10.1016/0016-7037(94)90177-5

Reimer, P. J., Austin, W. E. N., Bard, E., Bayliss, A., Blackwell, P. G., Bronk Ramsey, C., et al. (2020). The IntCal20 northern Hemisphere radiocarbon age calibration curve (0–55 cal kBP). *Radiocarbon*, *62*(4), 725–757. https://doi.org/10.1017/RDC.2020.41

Reimer, P. J., Bard, E., Bayliss, A., Beck, J. W., Blackwell, P. G., Bronk Ramsey, C., et al. (2013). Intcal13 and Marine13 radiocarbon age calibration curves 0–50,000 years cal Bp. *Radiocarbon*, *55*(4), 1869–1887. https://doi.org/10.2458/azu_js_rc.55.16947

Riddell-Young, B., Rosen, J., Brook, E., Buizert, C., Martin, K., Lee, J., et al. (2023). Atmospheric methane variability through the Last Glacial Maximum and deglaciation mainly controlled by tropical sources. *Nature Geoscience*, *16*(12), 1174–1180. https://doi.org/10.1038/s41561-023-01332-x

Rosen, J. L. (2014). *Augmenting and interpreting ice core greenhouse gas records*. Oregon State University.

Sabino, M., Gustafsson, Ö., Wild, B., Semiletov, I. P., Dudarev, O. V., Ingrosso, G., & Tesi, T. (2024a). Organic carbon content, stable carbon isotope ratios, and lignin phenol fingerprint of terrestrial material deposited at the paleo-delta of the Lena River at the transition to the Preboreal [Dataset]. *PANGAEA*. https://doi.org/10.1594/PANGAEA.972409

Sabino, M., Gustafsson, Ö., Wild, B., Semiletov, I. P., Dudarev, O. V., Ingrosso, G., & Tesi, T. (2024b). Radiocarbon content and age of terrestrial material deposited at the paleo-delta of the Lena River at the transition to the Preboreal [Dataset]. *PANGAEA*. https://doi.org/10.1594/PANGAEA.972412

Schlitzer, R. (2023). Ocean data view. Retrieved from http://odv.awi.de

Schuur, E. A. G., Mcguire, A. D., Schädel, C., Grosse, G., Harden, J. W., Hayes, D. J., et al. (2015). Climate change and the permafrost carbon feedback. *Nature*, *520*(7546), 171–179. https://doi.org/10.1038/nature14338

Semiletov, I. P., Pipko, I. I., Shakhova, N. E., Dudarev, O. V., Pugach, S. P., Charkin, A. N., et al. (2011). Carbon transport by the Lena River from its headwaters to the Arctic Ocean, with emphasis on fluvial input of terrestrial particulate organic carbon vs. carbon transport by coastal erosion. *Biogeosciences*, *8*(9), 2407–2426. https://doi.org/10.5194/bg-8-2407-2011

Smith, S. L., O'Neill, H. B., Isaksen, K., Noetzli, J., & Romanovsky, V. E. (2022). The changing thermal state of permafrost. *Nature Reviews Earth & Environment*, *3*(1), 10–23. https://doi.org/10.1038/s43017-021-00240-1

Steffensen, J. P., Andersen, K. K., Bigler, M., Clausen, H. B., Dahl-Jensen, D., Fischer, H., et al. (2008). High-resolution Greenland ice core data show abrupt climate change happens in few years. *Science*, *321*(5889), 680–684. https://doi.org/10.1126/science.1157707

Strauss, J., Schirrmeister, L., Grosse, G., Fortier, D., Hugelius, G., Knoblauch, C., et al. (2017). Deep Yedoma permafrost: A synthesis of depositional characteristics and carbon vulnerability. *Earth-Science Reviews*, *172*(February), 75–86. https://doi.org/10.1016/j.earscirev.2017.07.007

Stuiver, M., & Polach, H. A. (1977). Discussion reporting of 14C data. *Radio*, *19*(3), 355–363. https://doi.org/10.1017/s0033822200003672

Taldenkova, E., Bauch, H. A., Stepanova, A., Strezh, A., Dem'yankov, S., & Ovsepyan, Y. (2008). Postglacial to Holocene history of the Laptev Sea continental margin: Palaeoenvironmental implications of benthic assemblages. *Quaternary International*, *183*(1), 40–60. https://doi.org/10.1016/j.quaint.2007.06.031

Tarasov, P. E., Bezrukova, E. V., & Krivonogov, S. K. (2009). Late Glacial and Holocene changes in vegetation cover and climate in southern Siberia derived from a 15 kyr long pollen record from Lake Kotokel. *Climate of the Past*, *5*(3), 285–295. https://doi.org/10.5194/cp-5-285-2009

Tarasov, P. E., Müller, S., Zech, M., Andreeva, D., Diekmann, B., & Leipe, C. (2013). Last glacial vegetation reconstructions in the extreme-continental eastern Asia: Potentials of pollen and n-alkane biomarker analyses. *Quaternary International*, *290–291*, 253–263. https://doi.org/10.1016/j.quaint.2012.04.007

Tarnocai, C., Canadell, J. G., Schuur, E. A. G., Kuhry, P., Mazhitova, G., & Zimov, S. (2009). Soil organic carbon pools in the northern circumpolar permafrost region. *Global Biogeochemical Cycles*, *23*(2), 1–11. https://doi.org/10.1029/2008GB003327

Tesi, T., Muschitiello, F., Smittenberg, R. H., Jakobsson, M., Vonk, J. E., Hill, P., et al. (2016). Massive remobilization of permafrost carbon during post-glacial warming. *Nature Communications*, *7*(1), 13653. https://doi.org/10.1038/ncomms13653

Tesi, T., Semiletov, I., Dudarev, O., Andersson, A., & Gustafsson, Ö. (2016). Matrix association effects on hydrodynamic sorting and degradation of terrestrial organic matter during cross-shelf transport in the Laptev and East Siberian shelf seas. *Journal of Geophysical Research: Biogeosciences*, *121*(3), 731–752. https://doi.org/10.1002/2015JG003067

Tesi, T., Semiletov, I., Hugelius, G., Dudarev, O., Kuhry, P., & Gustafsson, Ö. (2014). Composition and fate of terrigenous organic matter along the Arctic land-ocean continuum in East Siberia: Insights from biomarkers and carbon isotopes. *Geochimica et Cosmochimica Acta*, *133*, 235–256. https://doi.org/10.1016/j.gca.2014.02.045

Tipple, B. J., & Pagani, M. (2007). The early origins of terrestrial C_4 photosynthesis. *Annual Review of Earth and Planetary Sciences*, *35*(1), 435–461. https://doi.org/10.1146/annurev.earth.35.031306.140150

Treat, C. C., Jones, M. C., Brosius, L., Grosse, G., Walter Anthony, K., & Frolking, S. (2021). The role of wetland expansion and successional processes in methane emissions from northern wetlands during the Holocene. *Quaternary Science Reviews*, *257*, 106864. https://doi.org/10.1016/j.quascirev.2021.106864

Treat, C. C., Kleinen, T., Broothaerts, N., Dalton, A. S., Dommaine, R., Douglas, T. A., et al. (2019). Widespread global peatland establishment and persistence over the last 130,000 y. *Proceedings of the National Academy of Sciences of the United States of America*, *116*(11), 4822–4827. https://doi.org/10.1073/pnas.1813305116

Treat, C. C., Natali, S. M., Ernakovich, J., Iversen, C. M., Lupascu, M., Mcguire, A. D., et al. (2015). A pan-Arctic synthesis of CH_4 and CO_2 production from anoxic soil incubations. *Global Change Biology*, *21*(7), 2787–2803. https://doi.org/10.1111/gcb.12875

Turetsky, M. R., Abbott, B. W., Jones, M. C., Anthony, K. W., Olefeldt, D., Schuur, E. A. G., et al. (2020). Carbon release through abrupt permafrost thaw. *Nature Geoscience*, *13*(2), 138–143. https://doi.org/10.1038/s41561-019-0526-0

Tveit, A. T., Urich, T., Frenzel, P., & Svenning, M. M. (2015). Metabolic and trophic interactions modulate methane production by Arctic peat microbiota in response to warming. *Proceedings of the National Academy of Sciences of the United States of America*, *112*(19), E2507–E2516. https://doi.org/10.1073/pnas.1420797112

van Winden, J. F., Reichart, G. J., McNamara, N. P., Benthien, A., & Damsté, J. S. S. (2012). Temperature-induced increase in methane release from peat bogs: A mesocosm experiment. *PLoS One*, *7*(6), 4–8. https://doi.org/10.1371/journal.pone.0039614

Vonk, J. E., Sanchez-Garca, L., Van Dongen, B. E., Alling, V., Kosmach, D., Charkin, A., et al. (2012). Activation of old carbon by erosion of coastal and subsea permafrost in Arctic Siberia. *Nature*, *489*(7414), 137–140. https://doi.org/10.1038/nature11392

Wakeham, S. G., Canuel, E. A., Lerberg, E. J., Mason, P., Sampere, T. P., & Bianchi, T. S. (2009). Partitioning of organic matter in continental margin sediments among density fractions. *Marine Chemistry*, *115*(3–4), 211–225. https://doi.org/10.1016/j.marchem.2009.08.005

Walter, K. M., Edwards, M. E., Grosse, G., Zimov, S. A., & Chapin, F. S. (2007). Thermokarst lakes as a source of atmospheric CH_4 during the last deglaciation. *Science*, *318*(5850), 633–636. https://doi.org/10.1126/science.1142924

Walter Anthony, K. M., Zimov, S. A., Grosse, G., Jones, M. C., Anthony, P. M., Iii, F. S. C., et al. (2014). A shift of thermokarst lakes from carbon sources to sinks during the Holocene epoch. *Nature*, *511*(7510), 452–456. https://doi.org/10.1038/nature13560

Wang, Y., Guo, Y., Wang, X., Song, C., Song, Y., Liu, Z., et al. (2023). Mineral protection controls soil organic carbon stability in permafrost wetlands. *Science of the Total Environment*, *869*(August 2022), 161864. https://doi.org/10.1016/j.scitotenv.2023.161864

Wild, B., Andersson, A., Bröder, L., Vonk, J., Hugelius, G., McClelland, J. W., et al. (2019). Rivers across the Siberian Arctic unearth the patterns of carbon release from thawing permafrost. *Proceedings of the National Academy of Sciences of the United States of America*, *116*(21), 10280–10285. https://doi.org/10.1073/pnas.1811797116

Williams, C. J., Yavitt, J. B., Wieder, R. K., & Cleavitt, N. L. (1998). Cupric oxide oxidation products of northern peat and peat-forming plants. *Canadian Journal of Botany*, *76*(1), 51–62. https://doi.org/10.1139/cjb-76-1-51

Winterfeld, M., Goñi, M. A., Just, J., Hefter, J., & Mollenhauer, G. (2015). Characterization of particulate organic matter in the Lena River delta and adjacent nearshore zone, NE Siberia—Part 2: Lignin-derived phenol compositions. *Biogeosciences*, *12*(7), 2261–2283. https://doi.org/10.5194/bg-12-2261-2015

Winterfeld, M., Laepple, T., & Mollenhauer, G. (2015). Characterization of particulate organic matter in the Lena River delta and adjacent nearshore zone, NE Siberia—Part I: Radiocarbon inventories. *Biogeosciences*, *12*(12), 3769–3788. https://doi.org/10.5194/bg-12-3769-2015

Winterfeld, M., Mollenhauer, G., Dummann, W., Köhler, P., Lembke-Jene, L., Meyer, V. D., et al. (2018). Deglacial mobilization of pre-aged terrestrial carbon from degrading permafrost. *Nature Communications*, *9*(1), 3666. https://doi.org/10.1038/s41467-018-06080-w

Yergeau, E., Hogues, H., Whyte, L. G., & Greer, C. W. (2010). The functional potential of high Arctic permafrost revealed by metagenomic sequencing, qPCR and microarray analyses. *ISME Journal*, *4*(9), 1206–1214. https://doi.org/10.1038/ismej.2010.41

Zech, M., Andreev, A., Zech, R., Müller, S., Hambach, U., Frechen, M., & Zech, W. (2010). Quaternary vegetation changes derived from a loess-like permafrost palaeosol sequence in northeast Siberia using alkane biomarker and pollen analyses. *Boreas*, *39*(3), 540–550. https://doi.org/10.1111/j.1502-3885.2009.00132.x

Zhang, T., Frauenfeld, O. W., Serreze, M. C., Etringer, A., Oelke, C., McCreight, J., et al. (2005). Spatial and temporal variability in active layer thickness over the Russian Arctic drainage basin. *Journal of Geophysical Research D: Atmospheres*, *110*(16), 1–14. https://doi.org/10.1029/2004JD005642

Zhang, X., Bianchi, T. S., Cui, X., Rosenheim, B. E., Ping, C. L., Hanna, A. J. M., et al. (2017). Permafrost organic carbon mobilization from the watershed to the Colville River delta: Evidence from ^{14}C ramped pyrolysis and lignin biomarkers. *Geophysical Research Letters*, *44*(22), 11491–11500. https://doi.org/10.1002/2017GL075543

Zona, D., Gioli, B., Commane, R., Lindaas, J., Wofsy, S. C., Miller, C. E., et al. (2016). Cold season emissions dominate the Arctic tundra methane budget. *Proceedings of the National Academy of Sciences of the United States of America*, *113*(1), 40–45. https://doi.org/10.1073/pnas.1516017113

References From the Supporting Information

Bauch, H. A., Erlenkeuser, H., Bauch, D., Mueller-Lupp, T., & Taldenkova, E. (2004). Stable oxygen and carbon isotopes in modern benthic foraminifera from the Laptev Sea shelf: Implications for reconstructing proglacial and profluvial environments in the Arctic. *Marine Micropaleontology*, *51*(3–4), 285–300. https://doi.org/10.1016/j.marmicro.2004.01.002

Blockley, S. P. E., Bronk Ramsey, C., Lane, C. S., & Lotter, A. F. (2008). Improved age modelling approaches as exemplified by the revised chronology for the Central European varved lake Soppensee. *Quaternary Science Reviews*, *27*(1–2), 61–71. https://doi.org/10.1016/j.quascirev.2007.01.018

Klemann, V., Heim, B., Bauch, H. A., Wetterich, S., & Opel, T. (2015). Sea-Level evolution of the Laptev Sea and the East Siberian Sea since the last glacial maximum. *Arktos*, *1*(1), 1–8. https://doi.org/10.1007/s41063-015-0004-x

Reimer, P. J., Brown, T. A., & Reimer, R. W. (2004). Discussion: Reporting and calibration of post-bomb 14C data. *Radiocarbon*, *46*(3), 1299–1304. https://doi.org/10.1017/S0033822200033154